AD-A087 028   PHYSICAL DYNAMICS INC LA JOLLA CALIF   F/G 4/1
                STABILITY OF BOUNDARY LAYER FLOW.(U)
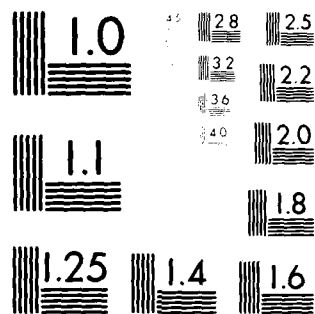   MAR 80   B E FREEMAN, L E HAUSER   N00173-79-C-0302
UNCLASSIFIED   PD-LJ-80-220   NL

END
DATE
FILMED
9-80
DTIC

MICROCOPY RESOLUTION TEST CHART

NATIONAL BUREAU OF STANDARDS 1963 A
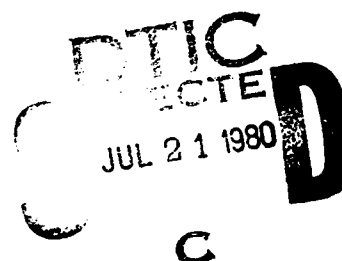
LEVEL

PD-LJ-80-220

PD INC. physical dynamics, inc.

STABILITY OF BOUNDARY LAYER FLOW

B. E. Freeman

L. E. Hauser

DTIC
ELECTE
JUL 21 1980

C

Physical Dynamics, Inc.
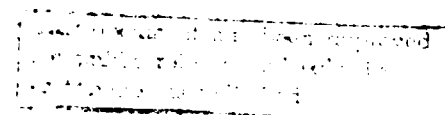Post Office Box 1883
La Jolla, CA 92038

March 1980

Final Report for the Period
11 September 1979 - 31 January 1980

Contract No. N00173-79-C-0302

Prepared For:

Naval Research Laboratory
4555 Overlook Avenue, SW
Washington, DC 20375

80   4   17   088

REPORT DOCUMENTATION PAGE		READ INSTRUCTIONS BEFORE COMPLETING FORM
1. REPORT NUMBER	2. GOVT ACCESSION NO. AD-A087028	3. RECIPIENT'S CATALOG NUMBER
4. TITLE (and Subtitle) STABILITY OF BOUNDARY LAYER FLOW		5. TYPE OF REPORT & PERIOD COVERED Final Report. 11 Sept 1979-31 Jan 1980
		6. PERFORMING ORG. REPORT NUMBER PD-LJ-80-220
7. AUTHOR(s) B. E. Freeman L. E. Hauser		8. CONTRACT OR GRANT NUMBER(s) N00173-79-C-0302
9. PERFORMING ORGANIZATION NAME AND ADDRESS Physical Dynamics, Inc. P.O. Box 1883 La Jolla, CA 92038		10. PROGRAM ELEMENT, PROJECT, TASK AREA & WORK UNIT NUMBERS
11. CONTROLLING OFFICE NAME AND ADDRESS Naval Research Laboratory 4555 Overlook Avenue, SW Washington, D.C. 20375		12. REPORT DATE March 1980
		13. NUMBER OF PAGES 87
14. MONITORING AGENCY NAME & ADDRESS(if different from Controlling Office)		15. SECURITY CLASS. (of this report) UNCLASSIFIED
		15a. DECLASSIFICATION DOWNGRADING SCHEDULE

16. DISTRIBUTION STATEMENT (of this Report)

17. DISTRIBUTION STATEMENT (of the abstract entered in Block 20, if different from Report)

18. SUPPLEMENTARY NOTES

19. KEY WORDS (Continue on reverse side if necessary and identify by block number)

Atmospheric Stability
Marine Boundary Layer Modeling
Linear Perturbation Analysis
Radar Surface Ducting
Atmospheric internal wave propagation

Incompressible Stratified Fluid Flow
Generalized Eigenvalue Problem

20. ABSTRACT (Continue on reverse side if necessary and identify by block number)

A technique is developed and applied for the evaluation of conditions under which marine boundary layers are unstable, and for computing the rate of growth of unstable motions. Linear perturbation equations are formulated which account for influence of wind shear, static stability, Coriolis force, turbulent diffusion, large-scale convergence, and geostrophic wind on linear stability. The mean quantities can be prescribed by analytic functions or supplied as numerical tables derived either from observed/specified data or a boundary layer model.

DD FORM 1473

Abstract. Cont.
The linearized model is solved as a generalized eigenvalue problem. Related cal-
culations with the SIGMET code are discussed, including radar properties of the
marine boundary layer.

Accession For .

NTIS GRA&I

DDC TAB

Unannounced

Justification

By

Distribution/

Availability Codes

Avail and/or

special

Dist

A

TABLE OF CONTENTS

INTRODUCTION

This document constitutes the final report of the second phase of
an investigation into convection in the marine atmosphere and into topics
pertaining to radar sensing of the atmosphere. In a short introductory
phase reported in the contract final report (Freeman 1979), we reviewed
relevant theoretical models of marine convection, surveyed the climato-
logical frequency of convection in the North Atlantic, and offered recom-
mendations on the modelling of triggered convection.

The current investigation has also had a limited scope of study;
the principal objective is to develop a technique for evaluating the
conditions under which boundary layers are unstable and for computing the
rate of growth of unstable motions. In recognition of the limited time
and funds available for this study we restricted our considerations to
simple models of the boundary layer, which can be evaluated without large
computer expense and complication. Nevertheless, it has been possible to
include in this framework all of the physical effects which can contribute
to the perturbed motion of the marine boundary layer. We take into account
the influence on linear stability of wind shear, static stability, Coriolis
force, turbulent diffusion, large-scale convergence, and the geostrophic
wind. A procedure has been developed for solving the linear perturbation
equations to obtain the complex eigenvalues and eigenfunctions correspond-
ing to a given unperturbed state of the boundary layer. The equations are
sufficiently general that realistic profiles of wind speed, density, and
diffusivity can be accomodated. We have provided alternative sources of
the profiles of mean quantities; they can be prescribed as analytic
functions, or they can be supplied as numerical tables derived either from
data or from a boundary layer model.

In our report to follow we describe this new computational technique and the results obtained with it. We also report on related calculations with the boundary layer computer code SIGMET, some studies of radar properties of the marine boundary layer, including ducting, and an investigation of atmospheric internal wave propagation.

The report is divided into four sections. In Section A we consider the mean structure of the boundary layer as displayed by the SIGMET computer code; stability of the boundary layer is discussed in Section B, where formulation, mathematical implementation, and numerical studies are presented. This section contains the major development of the study. In Section C, radar properties of the marine atmosphere are reviewed and in Section D a study of atmospheric internal wave propagation is reported. We believe it should be possible to associate radar surface ducting and internal wave activity with other properties of the marine atmosphere.

A.   MEAN STRUCTURE OF THE MARINE BOUNDARY LAYER

One of the capabilities which we require for the analysis of the boundary
layer is a description of the profiles of temperature, humidity, wind field,
and diffusivity. These quantities evolve through diurnal and inertial cycles
in response to external forcing parameters, such as sea surface temperature,
geostrophic wind, large-scale convergence or divergence of the horizontal
wind, and short- and long-wave radiation. They are also influenced by initial
conditions of atmospheric temperature, humidity, and wind field. In response
to these quantities the boundary layer changes with time as determined
by the Navier-Stokes equations and an approximation (based on second-order
closure) to the fields of several second-order variance and covariance
quantities formed from turbulent fluctuations.

The above-described model determines the laminar boundary layer in
terms of the average or unperturbed profiles of the atmosphere. Deviations
from the mean motion have been parameterized in terms of the turbulence
description as they affect the mean motion itself. This model is required
as a starting point for a more detailed model (see Section B) which describes
the response of the laminar layer to small perturbations. It is also the
starting point for the calculation of derived profile quantities (see Section
C) which characterize the propagation and scattering of microwaves in
the atmospheric boundary layer.

The unperturbed boundary layer is described by the appropriately
averaged Navier-Stokes equations. These are given in Eq. B-2 and in more
detail in an appendix to our proposal to the Naval Research Laboratory
(Freeman, 1978). In the latter report the formulation of the SIGMET
computer code embodying these equations is also described and several examples

of calculations with the code are presented.

In support of the current investigation we have carried out several additional calculations of the marine boundary layer with SIGMET. These calculations have been used as input data for the stability calculations of Section B and to provide the mean profiles from which the microwave modified refraction coefficient and structure function were calculated in Section C. The initial data for the calculation are shown in Fig. A-1, and the profiles of velocity, humidity and potential temperature at a time (0108 local time) eighteen hours after the initial time are presented in Fig. A-2 through A-5.

Finally, we have incorporated the terms describing the large-scale convergence or divergence of the horizontal winds into SIGMET. This term can be prescribed as an arbitrary function of altitude. From it the vertical velocity of the air column is calculated, which, in turn, determines the vertical advection terms. Applications of this version of SIGMET will be made at a later time.
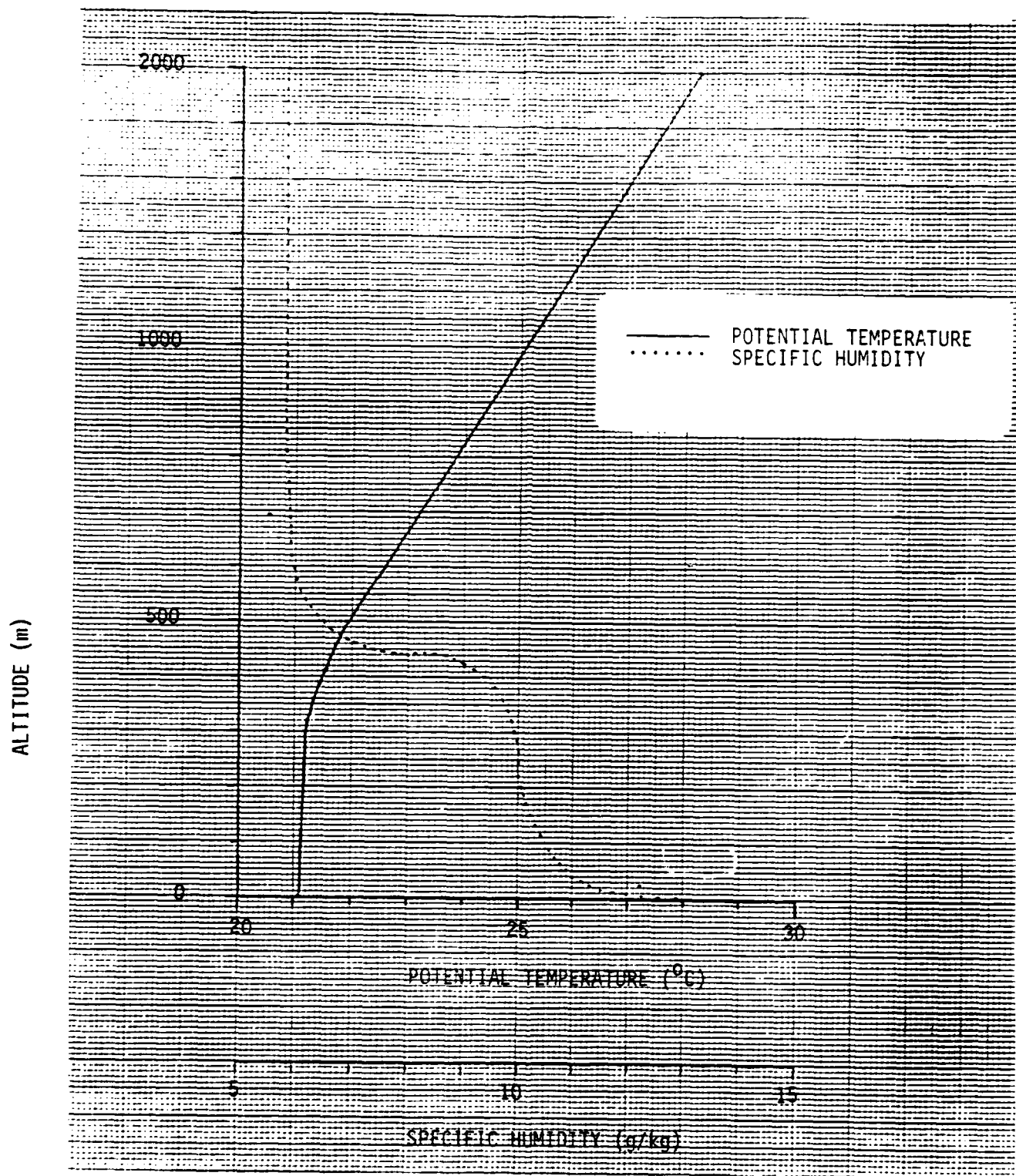
FIGURE A-1. Initial potential temperature and specify humidity profiles used for a SIGMET atmospheric boundary layer calculation. Local time = 0108 hours.

FIGURE A-2. SIGMET-calculated u-velocity field as a function of altitude at local time = 0108 hours.

FIGURE A-3. SIGMET-calculated v-velocity field as a function of altitude
at local time = 0108 hours.

FIGURE A-4. SIGMET-calculated specific humidity (g/g) as a function of altitude at local time = 0108 hours.

FIGURE A-5.   SIGMET-calculated potential temperature as a function of altitude at local time = 0108 hours.
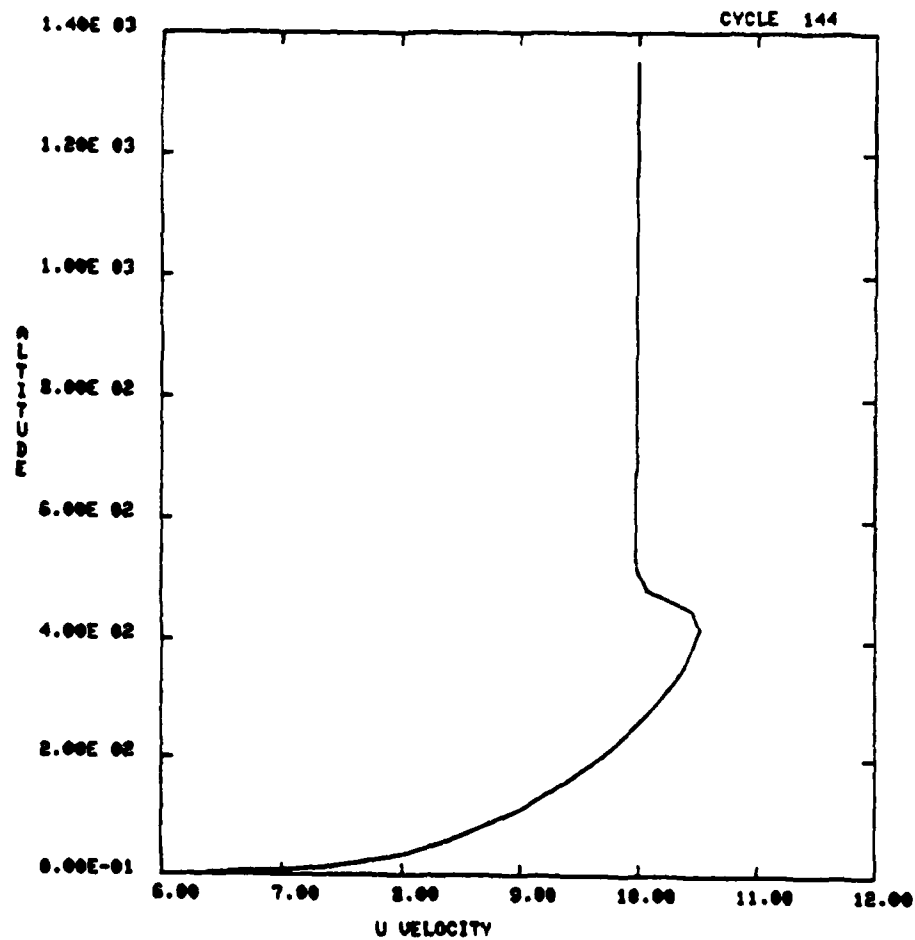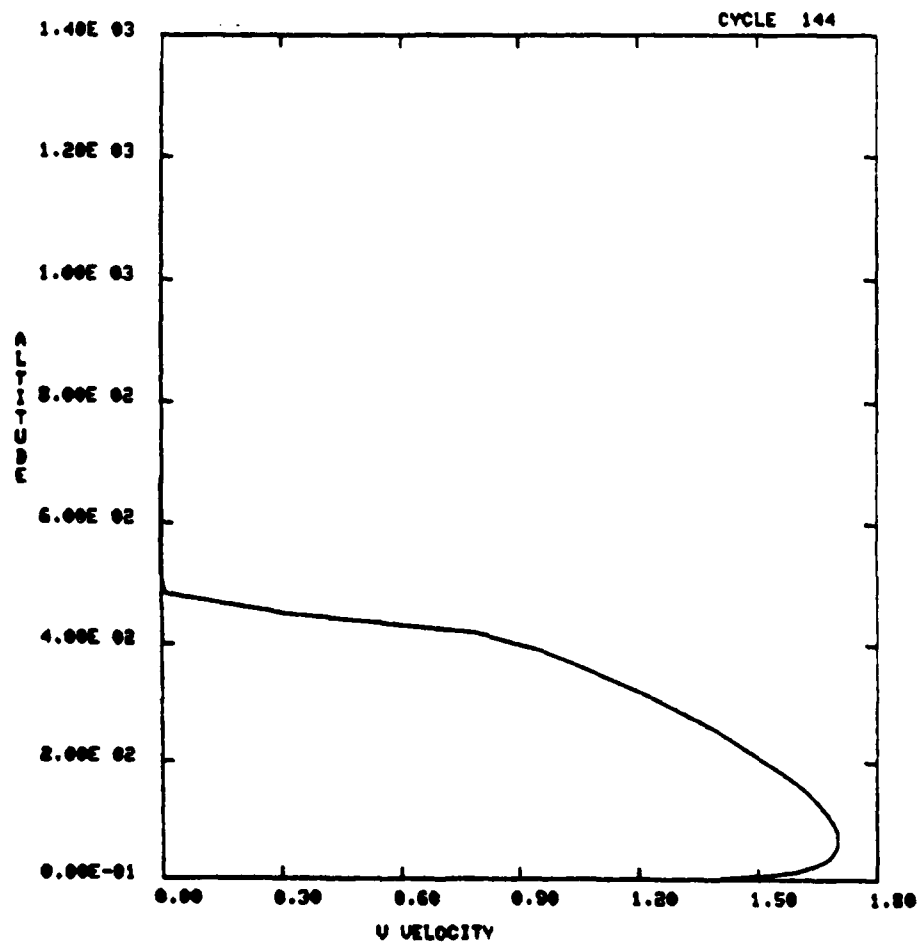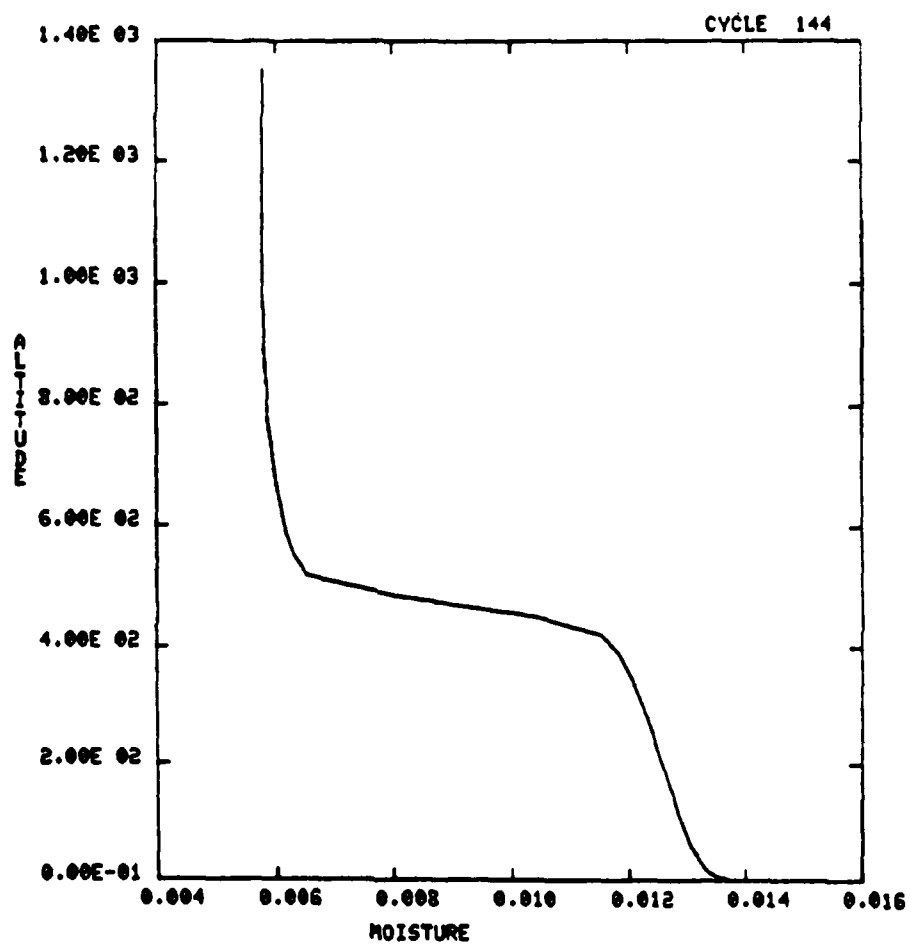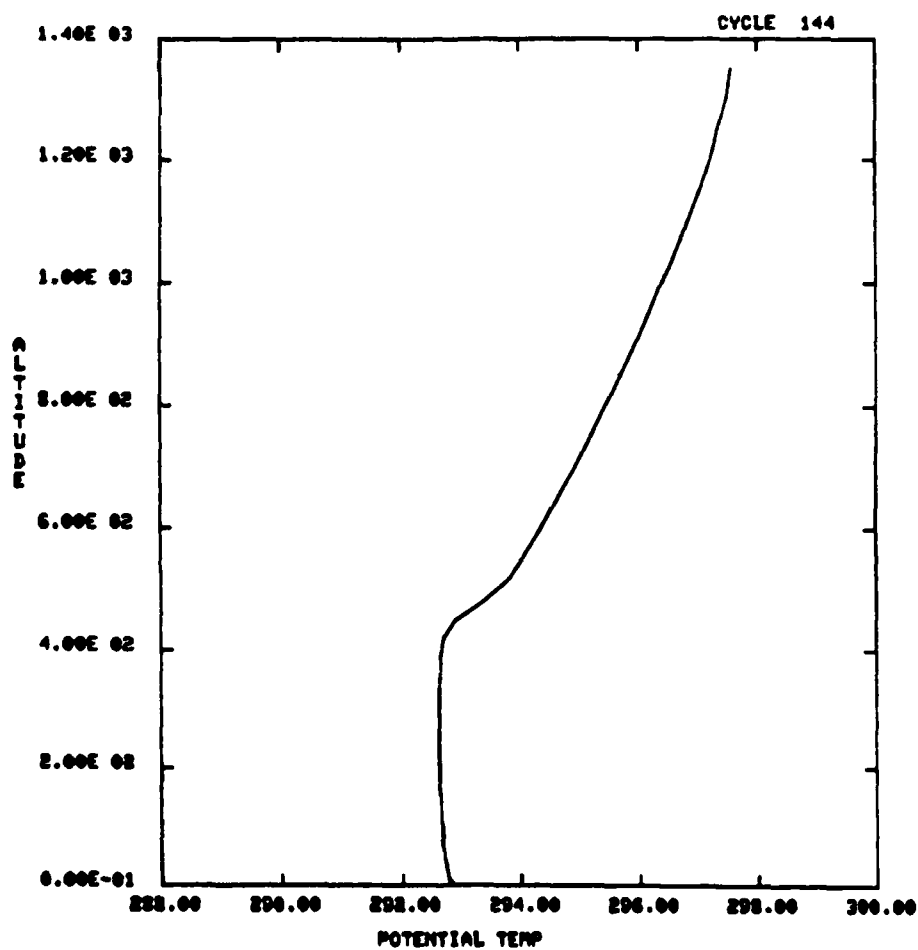
B. STABILITY OF BOUNDARY LAYER FLOW

In reviewing literature citations to determine what physical and mathematical approximations have been investigated, we found several studies of free convection (without wind shear) and others of shear instability in a neutrally stable atmosphere. The dependences of diffusivity and wind on altitude were highly idealized, and the role of a time-dependent unperturbed state had received little attention.

We have formulated the perturbation problem more generally to take account of these simplications. The perturbation equations are consistent with those solved by the computer code SIGMET which evaluates the evolution of profiles of wind, temperature, humidity, etc., in a turbulent boundary layer. These perturbations may be unstable; the degree of instability depends in general on external parameters, such as heat flux and geostrophic wind, and on the wavelength and direction of the perturbation. For each such combination a number of vertical modes are permissible.

The initial mathematical and numerical formulation was chosen to facilitate checking with previously obtained results and to permit assessment of the accuracy of the numerical solution. We assume for this purpose that the unperturbed state is steady and that the parameters derived from the unperturbed solution are provided on a finite grid of representative altitudes, as is the case using SIGMET. These points are not necessarily equally spaced. Since the coefficients are independent of time, we may assume that the time dependence of the perturbation amplitude corresponds to a constant phase speed. If the phase speed is real, the perturbation is a freely traveling wave (for example, an internal wave), but if there is an imaginary component, the wave is either damped or amplified. The evaluation of the complex phase speed (or frequency)

constitutes the basic problem of determining the linear perturbation solution. In the above formulation the solution is expressible as a matrix eigenvalue problem containing complex coefficients. The number of modes is determined by the number of altitude intervals; the higher modes of the continuous problem are suppressed by the finite difference representation. The eigenfunctions corresponding to a given eigenvalue provide the altitude dependence of the linear perturbation.

In the following sections the formulation of the incompressible, steady state linear stability problem is described. The calculation takes into account the effects of wind shear, atmospheric stability, large-scale pressure gradient and convergence, the Coriolis force and turbulent diffusion; these are included in the equations given in Section B-1. The differential equations contain derivatives of order four and lower; in Section B-2 these derivatives are approximated by difference equations of order four. The SIGMET spatial grid is not uniform in vertical spacing in order to provide higher resolution near the surface where the wind shear is large; we account for this nonuniformity by employing a coordinate transformation described in Section B-3. Boundary conditions and methods of solution of the complex matrix eigenvalue equations are presented in Sections B-4 and B-5. The resulting computer code (PERT) has been used to evaluate the stability of a large number of representative boundary layer flows. To test the correctness and accuracy of the solutions, comparisons were made with several reported stability analyses; these are discussed in Section B-6. A large number of parameters governing stability of atmospheric flows can be explored with the PERT computer code. In Section B-7 some of these have been investigated, including the simultaneous effects of static stability, wind shear, Coriolis force, and large-scale

11

divergence. We also present calculations based on the unperturbed

boundary flow derived from the SIGMET code. In Section B-8 we summarize

the status of linear stability analyses.

B.1 The Equations

The Navier-Stokes equations for an incompressible stratified fluid take into account the conservation of momentum in a viscous fluid and the equation for the conservation of mass in the presence of diffusion. These equations also include the effect of the Coriolis force in addition to the pressure in the fluid. In a fixed coordinate system x (positive eastward), y (positive northward), and z (positive vertically upward) the equations are

$$\frac{\partial U}{\partial t} + U\frac{\partial U}{\partial x} + V\frac{\partial U}{\partial y} + W\frac{\partial U}{\partial z} - fV + f'W + \frac{1}{\rho}\frac{\partial P}{\partial x} = \nabla \cdot (K\nabla U),$$

$$\frac{\partial V}{\partial t} + U\frac{\partial V}{\partial x} + V\frac{\partial V}{\partial y} + W\frac{\partial V}{\partial z} + fU + \frac{1}{\rho}\frac{\partial P}{\partial y} = \nabla \cdot (K\nabla V),$$

$$\frac{\partial W}{\partial t} + U\frac{\partial W}{\partial x} + V\frac{\partial W}{\partial y} + W\frac{\partial W}{\partial z} - f'U - \frac{1}{\rho}\frac{\partial P}{\partial z} + g = \nabla \cdot (K\nabla W),$$

$$\frac{\partial \rho}{\partial t} + U\frac{\partial \rho}{\partial x} + V\frac{\partial \rho}{\partial y} + W\frac{\partial \rho}{\partial z} = \nabla \cdot (K'\nabla \rho),$$

$$\frac{\partial U}{\partial x} + \frac{\partial V}{\partial y} + \frac{\partial W}{\partial z} = 0. \qquad\qquad \text{B-(1)}$$

Equation B-(1) contains the wind velocity components (U, V, W), the pressure P, the density ρ, the Coriolis parameters $f = 2\Omega\sin\phi$, and $f' = 2\Omega\cos\phi$, and the (primarily turbulent) viscosity K and diffusivity K'.

Our approach is to consider solutions to B-(1) which represent horizontally stratified boundary layer flow (the unperturbed solution) and to investigate its linear stability against perturbations involving horizontal inhomogeneity. The equations for the perturbations are linearized by neglecting all nonlinear terms.

The mean flow equations neglect all horizontal variations except for an assumed large-scale (synoptic) pressure gradient and convergence

13

or divergence of the horizontal wind speed. These terms, which can be functions of altitude, are assumed to be derivable from synoptic weather data. Including these terms, the mean flow equations are

$$\frac{\partial \overline{U}}{\partial t} + \overline{W}\frac{\partial \overline{U}}{\partial z} - f\ (\overline{V}-V_g) + f'W = \frac{\partial}{\partial z}\ (K\ \frac{\partial \overline{U}}{\partial z}),$$

$$\frac{\partial \overline{V}}{\partial t} + \overline{W}\frac{\partial \overline{V}}{\partial z} + f\ (\overline{U}-U_g) = \frac{\partial}{\partial z}\ (K\ \frac{\partial \overline{V}}{\partial z})$$

$$\frac{\partial \overline{W}}{\partial t} + \overline{W}\frac{\partial \overline{W}}{\partial z} - f'\overline{U} + \frac{1}{\rho}\ \frac{\partial \overline{P}}{\partial z} + g = \frac{\partial}{\partial z}\ (K\ \frac{\partial \overline{W}}{\partial z}),$$

$$\frac{\partial \overline{\rho}}{\partial t} + \overline{W}\ \frac{\partial \overline{\rho}}{\partial z} = \frac{\partial}{\partial z}\ (K'\ \frac{\partial \overline{\rho}}{\partial z}),$$

$$\frac{\partial \overline{W}}{\partial z} = -\ D. \qquad\qquad\qquad B\text{-}(2)$$

In the third equation for the vertical component of momentum it is permissible to neglect the terms containing the velocity because over a flat surface they are very small compared with the acceleration of gravity g, and the term containing the hydrostatic pressure gradient $\frac{\partial \overline{P}}{\partial z}$. In this (hydrostatic) approximation the vertical momentum equation becomes

$$\frac{\partial \overline{P}}{\partial z} = -\ \overline{\rho}g. \qquad\qquad\qquad B\text{-}(3)$$

The final equation gives the vertical wind speed by imposing the surface boundary condition $\overline{W} = 0$ and integrating the horizontal divergence $D = \frac{\partial \overline{U}}{\partial x} + \frac{\partial \overline{V}}{\partial y}$, which is a known function of altitude. Other quantities appearing in B-(2) are the geostrophic wind components

$$(U_g, V_g) = (- \frac{1}{\bar{\rho}f} \frac{\partial \bar{P}}{\partial y} , \frac{1}{\bar{\rho}f} \frac{\partial \bar{P}}{dx}),$$

assumed to be known functions of altitude. The turbulent viscosity K and diffusivity K' are determined by appeal to turbulence theory. In 1-D SIGMET, which solves the above system of equations, a set of auxiliary equations is solved to determine the turbulent diffusivities. These are obtained by second order closure hypotheses; a prognostic equation for the turbulent kinetic energy and algebraic equations for derived turbulent quantities result. In the following applications we are able to use the 1-D SIGMET code to provide data on the mean flow solution, including the turbulent diffusivities. In doing so, we require a number of quantities (such as f, D, U_g, V_g, surface boundary conditions, etc.) which specify the problem in terms of local and synotic parameters. Their values determine whether the unperturbed atmosphere is stable or unstable and the amount of wind shear and turning in the boundary layer. A more detailed description of the SIGMET formulation is given by Freeman (1978).

The mean flow solution described above will respond to a perturbation in accordance with the Navier-Stokes equations (1); the perturbation may grow, diminish or maintain constant amplitude depending on both the nature of the mean flow and of the perturbation itself. The perturbation is assumed to have a small enough amplitude that the governing equations may be linearized (neglecting terms of higher order than the first in the perturbation amplitudes). While the perturbation itself is a function of horizontal position, as well as altitude and time, the coefficients of the governing equations do not depend on horizontal position. For this reason, the perturbation may be assumed to be a sinusoidal function of the horizontal coordinate, x.

$$\psi = \psi_0 (z, \underline{k}, t) e^{i\underline{k} \cdot \underline{x}} \qquad\qquad \text{B-(4)}$$

where $\underline{k}$ is the vector horizontal wavenumber of the perturbation; a perturbation of more general horizontal dependence may be constructed by superposition of these solutions. For the assessment of stability the wavenumber vector $\underline{k} = (k_x, k_y)$ constitutes an additional parameter which must be sampled.

The time dependence of the solution $\psi_0(z,t)$ determines the stability of the perturbation. In general, the governing equations form an initial value problem; starting from a given amplitude, the solution will change with time in accordance with the perturbation equations themselves. The time dependence is simplified, however, if the coefficients of the perturbation equations are independent of time; such is the case when the solution for the mean flow forms a steady state, as in the case of the classical Ekman spiral. In general, the mean flow solution is not steady (due to diurnal oscillations, inertial oscillations, initial state of un-stable heating, etc.), but it is sufficiently convenient that we will make this assumption for the interim. Then we can write.

$$\psi_0(z, \underline{k}, t) = \psi_{00}(z, \underline{k}) e^{-i\omega t} \qquad\qquad \text{B-(5)}$$

and if we wish, the more general solution may be constructed by super-position.

We now carry out the derivation of the linearized equations govern-ing the perturbation. By subtraction of B-(2) from B-(1) and using B-(4) we obtain

$$\frac{\partial u}{\partial t} + i\,\underline{k}\cdot\overline{\underline{U}}\,u + \overline{W}\,u_z + w\,\overline{U}_z - f\left(v + \frac{\rho}{\rho}\,V_g\right) + f'w + \frac{ik_x}{\rho}\,p = k^2\,K_H^m\,u + (K_v^m\,u_z)_z \quad ,$$

$$\frac{\partial v}{\partial t} + i\,\underline{k}\cdot\overline{\underline{U}}\,v + \overline{W}\,v_z + w\,\overline{V}_z + f\left(u + \frac{\rho}{\rho}\,U_g\right) + \frac{ik_y}{\rho}\,p = -\,k^2\,K_H^m\,v + (K_v^m\,v_z)_z \quad ,$$

$$\frac{\partial w}{\partial t} + i\,\underline{k}\cdot\overline{U}\,w - Dw + \overline{W}\,w_z + \frac{\rho}{\rho}\,g + \frac{1}{\rho}\,p_z = -\,k^2\,K_H^m\,w + (K_v^m\,w_z)_z \quad ,$$

$$\frac{\partial\rho}{\partial t} + i\,\underline{k}\cdot\overline{U}\,\rho + \overline{W}\,\rho_z + w\,\overline{\rho}_z = -\,k^2\,K_H^H\,\rho + (K_v^H\,\rho_z)_z \quad ,$$

$$i\,\underline{k}\cdot\underline{u} + w_z = 0 \quad . \hspace{4cm} \text{B-(6)}$$

In the perturbation equation for w the small term involving f' was neg-
lected and the hydrostatic approximation B-(3) was used to eliminate the
vertical component of the mean pressure gradient.

The equations B-(6), together with boundary conditions, constitute
the linear perturbation problem for an incompressible fluid in a very
general form. The coefficients may be quite arbitrary functions of
altitude and time. While we plan to return to this general problem in the
future, for the interim we assume that the coefficients do not depend on
time, so that the solution form B-(5) is applicable. The frequency ω
constitutes a complex eigenvalue whose value is determined by requiring
the solution for a given wavenumber vector $\underline{k}$ to satisfy the prescribed
boundary conditions. For each value of $\underline{k}$ there is a multiplicity of
eigenvalues; they are distinguished from each other by a mode index
corresponding to the number of nodes of the solution in the altitude
range.

Let us now substitute the time dependence of B-(5) into B-(6) and
rearrange the equations for easier solution. The first two equations of

B-(6) are combined to form components parallel to $\underline{k}$ ($\mu = \underline{k} \cdot \underline{u}$) and perpendicular to $\underline{k}$ ($\eta = k_y u - k_x v$)

$$(K_v^M \mu_z)_z - \overline{W} \mu_z + [i(\omega - \underline{k} \cdot \underline{\overline{U}}) - k^2 K_H^M] \mu - \underline{k} \cdot \underline{\overline{U}}_z w - \frac{ik^2}{\overline{\rho}} P - f'k_x w$$

$$- f [\eta + \frac{1}{\overline{\rho}} (k_y U_g - k_x V_g) \rho] = 0 \quad ,$$

$$(K_v^M \eta_z)_z - \overline{W} \eta_z + [i(\omega - \underline{k} \cdot \underline{\overline{U}}) - k^2 K_H^M] \eta - (k_y \overline{U} - k_x \overline{V})_z w - f'k_y w$$

$$+ f [\mu + \frac{1}{\overline{\rho}} \underline{k} \cdot \underline{U}_g \rho] = 0 \quad . \qquad\qquad \text{B-(7)}$$

These equations are coupled together only by the Coriolis term. The equation for η does not contain the pressure.

It is now convenient to eliminate the pressure from the w equation by using the first of B-(7); we also eliminate μ by using the last equation of B-(6). When we do this the order of the resulting equation is raised to the fourth. Rather than raise the order still higher, we solve simultaneous equations for η, ρ and w. The equations are (neglecting f')

$$(K_V^M \eta_z)_z - \overline{W} \eta_z + [i(\omega - \underline{k}\cdot\overline{\underline{U}}) - k^2 K_H^M] \eta + f \frac{\underline{k}\cdot\overline{\underline{U}}_z}{\overline{c}} \zeta$$

$$+ if_{w_z} - (k_y\overline{U} - k_x\overline{V})_z \, w = 0,$$

$$(K_V^H \zeta_z)_z - \overline{W} \zeta_z + [i(\omega - \underline{k}\cdot\overline{\underline{U}}) - k^2 K_H^H] \rho - \overline{\zeta}_z \, w = 0,$$

$$\frac{1}{\rho} [\, \overline{\rho} \, (K_V^M w_{zz})_z]_z - \overline{W} w_{zzz} + [i(\omega - \underline{k}\cdot\overline{\underline{U}}) - k^2 K_H^M + D - \frac{\overline{\rho}_z}{\rho} \overline{W}]w_{zz}$$

$$- k^2(K_V^M w_z)_z + \frac{\overline{\rho}_z}{\rho} [i(\omega - \underline{k}\cdot\overline{\underline{U}}) - k^2 K_H^M]\, w_z + k^2 \, (\overline{w} - (K_H^M)_z)w_z$$

$$+ [k^2 (k^2 K_H^M - D) + i(-k^2(\omega - \underline{k}\cdot\overline{\underline{U}}) + \frac{\overline{\rho}_z}{\rho} \underline{k}\cdot\overline{\underline{U}}_z + \underline{k}\cdot\overline{\underline{U}}_{zz})]w$$

$$+ \frac{if}{\overline{\rho}} (\overline{\rho} \, \eta)_z + \frac{if}{\overline{\rho}} [(k_y U_g - k_x V_g) \, \rho]_z + k^2 \frac{g}{\overline{\rho}} \rho = 0 \quad . \qquad \text{B-(8)}$$

To summarize, we have derived perturbation equations for a boundary layer
in which the unperturbed state contains an arbitrarily stratified density
and wind shear. Large-scale processes are represented by the geostrophic
wind and the horizontal divergence of the mean wind. We have included
Coriolis terms, but have assumed incompressibility. With these effects
taken into account the equations are considerably more general than have
been studied before. They include as special cases free convection,
internal wave propagation, Ekman spiral instability, etc. If the Coriolis
terms are omitted the η-equation need not be solved simultaneously with
those for w and ρ. The retention of geostrophic and divergence terms does
not greatly complicate the equations. The diffusion terms increase the
order of the equations; in general, the equivalent order of a single
equation is the eighth, but if the Coriolis term is zero the order is

recuced to sixth. The constant density (neutral stratification) problem is of sixth order, and becomes of fourth order when $f = 0$. Omitting ciffusion terms, the equations are of fifth order unless $\overline{W} = 0$ when they are of second order. For this last case the equations are readily solved by iteration of the solution of the second order equations as in ZMODE (Milder, 1973). It is thus apparent that the internal wave propagation problem (which is of second order) can be generalized to include geostrophic terms and unstable atmospheric stratification, as well as the effect of wind shear. Numerical solution of the equations could be accomplished by several different methods, of which the iterative integration method used in ZMODE has been alluded to. The method of time integration has also been mentioned. Each of these methods presents some difficulties; the iterative method would require generalization to higher order coupled equations as would the eigenvalue search procedure, while the time integration method suppresses modes with smaller eigenvalues. In the following sections a matrix solution technique is outlined. This method has the advantage that all eigenvalues are obtained without iteration, and accuracy is readily controlled.

B.2   Difference Equations

The matrix method of solution of B-(8) requires that difference
equations on a finite grid of points replace the differential equations.
When this has been accomplished the resulting system of linear coupled
algebraic equations can be expressed as a matrix equation for the vector
consisting of the unknown values of the three quantities r, c and w at
each of the altitude positions. Since the frequency ω enters into certain
terms of these equations as a linear factor, the complete set of equations
can be cast in the form of a generalized eigenvalue problem. In general,
the elements of the coefficient matrices are complex and the resulting
eigenvalues may be complex. The real part of the eigenvalue measures
the phase speed of the disturbance, while the imaginary part measures its
growth or decay rate. If the atmosphere is divided into I cells or grid
points the values of the unknown eigenvector $\underline{X}$ (consisting of n, c and w)
are 3I in number. The difference equations corresponding to B-(8) are of
the form

$$A\underline{X} = B\omega\underline{X} \quad , \qquad\qquad\qquad\qquad\qquad\qquad \text{B-(9)}$$

where A and B are square matrices of order 3I. The exact form of the co-
efficient matrices depends on the difference equations, on the order of
arrangement of the elements of the eigenvector, and on the boundary
conditions. In order to simplify the matrices (and facilitate partitioning
into IxI submatrices) the order of the eigenvector is chosen to be

$$\tilde{\underline{X}} = \{n_1, \ n_2 \ \cdot \ \cdot \ \cdot \ n_I, \ c_1, \ c_2 \ \cdot \ \cdot \ \cdot \ c_I, \ w_1, \ w_2 \ \cdot \ \cdot \ \cdot \ w_I\} \quad .$$

In this section the difference approximation to the differential expressions will be developed. We assume, at this time, that the independent variable X is divided into equal intervals ΔX such that $X_{max} - X_{min} = I\Delta X$; the center position of each interval is associated with the values η_i, ς_i and w_i. In the following section we consider the transformation from the altitude Z to X, such that the interval in Z is non-uniform, as required for accuracy in a planetary boundary layer calculation. Referring to B-(8), we note that the highest order of derivative is the fourth, which requires a minimum of five adjacent points for representation. This implies that at least one of the IxI submatrices will be pentadiagonal (containing non-zero values on the principal diagonal and two bordering diagonals above and two below it). We elect to represent lower order derivatives with a fourth order difference expression as well, since to do so will presumably increase the accuracy, will invoke a consistent order of difference approximation, and will not increase the number of non-zero matrix elements. Boundary conditions will affect the difference expressions at points immediately adjacent to the top and bottom boundaries and points one zone removed from them. In the interior of the mesh the fourth order centered difference approximations to the first four derivatives are

$$f^{(1)} \equiv \frac{df}{dx} \simeq \frac{f_{i-2} - 8f_{i-1} + 8f_{i+1} - f_{i+2}}{12 \, \Delta x} \quad ,$$

$$f^{(2)} \equiv \frac{d^2 f}{dx^2} \simeq \frac{-f_{i-2} + 16f_{i-1} - 30f_i + 16f_{i+1} - f_{i+2}}{12\Delta x^2} \quad ,$$

$$f^{(3)} \equiv \frac{d^3 f}{dx^3} \simeq \frac{-f_{i-2} + 2f_{i-1} - 2f_{i+1} + f_{i+2}}{2\Delta x^3} \quad ,$$

$$f^{(4)} \equiv \frac{d^4 f}{dx^4} \simeq \frac{f_{i-2} - 4f_{i-1} + 6f_i - 4f_{i+1} + f_{i+2}}{\Delta x^4} \quad , \qquad \text{B-(10)}$$

where the derivatives are evaluated at x_i and the subscript on the dependent function f_i denotes the position at which it is evaluated. The above expressions may be represented more concisely in matrix notation

$$\begin{pmatrix} f^{(0)} \\ f^{(1)} \\ f^{(2)} \\ f^{(3)} \\ f^{(4)} \end{pmatrix} = C^{-1} \begin{pmatrix} f_{i-2} \\ f_{i-1} \\ f_i \\ f_{i+1} \\ f_{i+2} \end{pmatrix} , \qquad \text{B-(11)}$$

where the coefficient matrix C^{-1}(5x5) is obtained from B-(10)

$$C^{-1} = \begin{pmatrix} 1 & 0 & 0 & 0 & 0 \\ 0 & (12\Delta x)^{-1} & & & 0 \\ 0 & 0 & (12\Delta x^2)^{-1} & & 0 \\ 0 & 0 & 0 & (2\Delta x^3)^{-1} & 0 \\ 0 & 0 & 0 & 0 & \Delta x^{-4} \end{pmatrix} \begin{pmatrix} 0 & 0 & 1 & 0 & 0 \\ 1 & -8 & 0 & 8 & -1 \\ -1 & 16 & -30 & 16 & -1 \\ -1 & 2 & 0 & -2 & 1 \\ 1 & -4 & 6 & -4 & 1 \end{pmatrix}$$

While it is quite straightforward to derive the expressions given in B-(10), it is desirable to formulate a general method for doing so which is also applicable at boundary positions. Consequently, the function and its derivatives are expressed in terms of neighboring values of the function. The quartic approximation is

$$f(x) = f_i + \sum_{j=1}^{4} a_j (x-x_i)^j \quad ,$$

in terms of which the derivatives at x_i are

$$f_i^{(k)} = k! \, a_k \quad .$$

We can now find the four unknown coefficients a_j by evaluating the function at $x = x_i + n\Delta x$ (the four neighboring positions),

$$f_{i+n} = f_i + \sum_{j=1}^{4} \frac{f^{(j)}}{j!} \Delta x^j \, n^j \quad , \qquad\qquad \text{B-(12)}$$

where $n = -2, -1, 0, +1, +2$. We have replaced a_j by the corresponding derivative, and now have five equations for the function and its four derivatives. When written as a matrix equation B-(12) becomes

$$\begin{pmatrix} f_{i-2} \\ f_{i-1} \\ f_i \\ f_{i+1} \\ f_{i+2} \end{pmatrix} = C \begin{pmatrix} f^{(0)} \\ f^{(1)} \\ f^{(2)} \\ f^{(3)} \\ f^{(4)} \end{pmatrix} \quad ,$$

where

$$C = \begin{pmatrix} 1 & -2 & 4 & -8 & 16 \\ 1 & -1 & 1 & -1 & 1 \\ 1 & 0 & 0 & 0 & 0 \\ 1 & 1 & 1 & 1 & 1 \\ 1 & 2 & 4 & 8 & 16 \end{pmatrix} \begin{pmatrix} 1 & 0 & 0 & 0 & 0 \\ 0 & \Delta x & 0 & 0 & 0 \\ 0 & 0 & \frac{\Delta x^2}{2} & 0 & 0 \\ 0 & 0 & 0 & \frac{\Delta x^3}{6} & 0 \\ 0 & 0 & 0 & 0 & \frac{\Delta x^4}{24} \end{pmatrix} . \qquad \text{B-(13)}$$

The inverse of C gives the desired coefficient matrix C^{-1} of B-(11).

It is now easy to write the C matrix by inspection; the C^{-1} matrix is obtained by numerical inversion, and subsequent operations are performed as matrix and vector products, resulting ultimately in the elements of the A and B matrices.

B.3   Coordinate Transformations

The finite difference intervals of the altitude Z are chosen as a function of altitude in the SIGMET boundary layer computer code. Since the mean wind shear is large near the surface, higher resolution near the surface results in greater computational efficiency. An analytic expression has been chosen which contains a linear and a logarithmic term, such that near the surface the wind velocity obeys the law of the wall. Our application of this transformation is based on the form chosen for the SIGMET computer code; it contains, in fact, two transformations. The first introduces a scaled pressure coordinate, σ, the purpose of which is to simplify boundary conditions in a multidimensional primitive variable calculation; for the present application this transformation is not essential and introduces some complication which would otherwise be absent. The second transformation generates a non-uniform mesh in the σ coordinate in order to improve resolution in the surface boundary layer; the latter transformation is useful for the perturbation equations as well as the equation of mean flow. To maintain compatibility with SIGMET we retain both of these transformations which are described below.

The sigma coordinate is defined in terms of the mean pressure $\overline{P}$,

$$\sigma = \frac{\overline{P} - \overline{P}_T}{\pi} \quad ,$$

where $\pi = \overline{P}_B - \overline{P}_T$, and $\overline{P}_B$ = mean pressure at the surface, and $\overline{P}_T$ = mean pressure at the top of the computational region. The σ coordinate has the range $0 \leq \sigma \leq 1$, where zero corresponds to the top of the mesh and unity to the surface. Using the hydrostatic relation B-(3) we obtain

$$\frac{d\zeta}{dz} = - \frac{g\zeta}{\pi} \quad .$$

B-(14)

The transformation to a non-uniform σ grid uses a log-linear relation

$$x = 1-\sigma + \alpha \ln (1-\sigma + \sigma_0) \quad ,$$

where α and σ_0 are parameters determining the extent and severity of the non-uniformity. We will require

$$\frac{dx}{d\sigma} = - (1 + \frac{\alpha}{1-\sigma + \sigma_0}) \quad .$$

B-(15)

The x-coordinate will be divided into uniform intervals $\Delta x = \dfrac{\alpha \ln[\sigma_0/(1+\sigma_0)]-1}{I}$. We now wish to express the Z-derivatives (up to order four) which appear in B-(8) in terms of x-derivatives; due to the uniform interval on X we may use the difference expressions, derived in Section B-2, to evaluate the X-derivatives.

$$\frac{d}{dz} = \frac{d\sigma}{dz} \frac{dx}{d\sigma} \frac{d}{dx} = \frac{g\rho}{\pi} (1 + \frac{\alpha}{1-\sigma + \sigma_0}) \frac{d}{dx} \quad .$$

B-(16)

Taking account of the dependence of the coefficient of B-(16) on σ, the higher derivates are obtained by successive application of the above formulae.

$$\frac{d^2}{dz^2} = (\frac{\alpha}{\tau})^2 \ \{[1 + \frac{\alpha}{1-\sigma + \sigma_0}]^2 \frac{d^2}{dx^2} - \frac{\alpha}{(1-\sigma + \sigma_0)^2} \ \frac{d}{dx} \ .$$

$$\frac{d^3}{dz^3} = (\frac{\alpha}{\tau})^3 \ \{[1 + \frac{\alpha}{1-\sigma + \sigma_0}]^3 \frac{d^3}{dx^3} - \frac{3\alpha}{(1-\sigma + \sigma_0)^2} \ [1 + \frac{\alpha}{1-\sigma + \sigma_0}] \frac{d^2}{dx^2} \ ,$$

$$+ \frac{2\alpha}{(1-\sigma + \sigma_0)^3} \ \frac{d}{dx}\} \ ,$$

$$\frac{d^4}{dz^4} = (\frac{\alpha}{\tau})^4 \ \{[1 + \frac{\alpha}{1-\sigma + \sigma_0}]^4 \frac{d^4}{dx^4} - \frac{6\alpha}{(1-\sigma + \sigma_0)^2} \ [1 + \frac{\alpha}{1-\sigma + \sigma_0}]^2 \frac{d^3}{dx^3}$$

$$+ [\frac{8\alpha}{(1-\sigma + \sigma_0)^3} \ (1 + \frac{\alpha}{1-\sigma + \sigma_0}) + 3 \ (\frac{\alpha}{(1-\sigma + \sigma_0)^2})^2] \frac{d^2}{dx^2} - \frac{6\alpha}{(1-\sigma + \sigma_0)^4} \ \frac{d}{dx}\} \ .$$

B-(17)

Clearly, equations B-(16) and B-(17) can be expressed as a matrix, relating the z-derivatives with the x-derivatives, having the form

$$\begin{pmatrix} f \\ f_z \\ f_{zz} \\ f_{zzz} \\ f_{zzzz} \end{pmatrix} = \begin{pmatrix} 1 & 0 & 0 & 0 & 0 \\ 0 & \alpha_{11} & 0 & 0 & 0 \\ 0 & \alpha_{21} & \alpha_{22} & 0 & 0 \\ 0 & \alpha_{31} & \alpha_{32} & \alpha_{33} & 0 \\ 0 & \alpha_{41} & \alpha_{42} & \alpha_{43} & \alpha_{44} \end{pmatrix} \begin{pmatrix} f^{(0)} \\ f^{(1)} \\ f^{(2)} \\ f^{(3)} \\ f^{(4)} \end{pmatrix} \ ,$$

B-(18)

where the coefficients α_{ij} are obtained in an obvious way from B-(16) and B-(17), and $f^{(j)} \equiv \frac{d^j}{dx^j}$ as before. Denoting the matrix of B-(18) by D, the $f^{(j)}$ vector can be evaluated from B-(11) to give

$$
\begin{pmatrix} f \\ f_z \\ f_{zz} \\ f_{zzz} \\ f_{zzz} \end{pmatrix} = DC^{-1} \begin{pmatrix} f_{i-2} \\ f_{i-1} \\ f_i \\ f_{i+1} \\ f_{i+2} \end{pmatrix}
$$

B-(19)

Finally, B-(19) can be multiplied by the vector consisting of the co-efficients of the derivatives of each of the variables η, ρ, w in the three equations of B-(8); the results are the vectors giving the elements on the pentadiagonals of the submatrices. For illustration, consider the simple example of the terms from the third equation of B-(8) containing η: if $(\eta_z + \frac{\bar{\rho}_z}{\bar{\rho}} \eta)$. The coefficients of η_i are given by the vector result-ing from $\{if \frac{\bar{\rho}_z}{\bar{\rho}}, if, 0, 0, 0\} DC^{-1}$. These coefficients are a function of altitude due to the height dependence of $\bar{\rho}_z$.

The above procedure is used to obtain all of the matrix coefficients in the interior of the matrix. Boundary conditions, however, must be invoked on zones near the boundaries. These affect the coefficients result-ing from the two zones adjacent to the top boundary and the two adjacent to the bottom boundary. These are derived in the next section.

B.4   Boundary Conditions

In Section 2 difference approximations were derived between the
derivatives entering the perturbation equations B-(8) and the values of
the function at mesh points. These relations involve values of the
function two intervals above and below as well as at the cell in question.
Clearly, at cells adjacent to or one cell removed from the boundaries
the difference expression B-(11) is not suitable because it would require
undefined values of the functions. At these locations, however, the
differential equations also require special treatment in the form of
boundary conditions describing physical conditions of the interaction of
the fluid and the boundary. These boundary conditions are often idealized
and simplified, corresponding in some cases to the necessity of truncating
a large region with an artificial boundary (such as the upper boundary
of the planetary boundary layer).

In this section we derive relations analogous to B-(11) which are
to replace B-(11) in the boundary cells. This is accomplished by modify-
ing the equations B-(12) which define the coefficients of the quartic
(and which, in turn, are proportional to the first four derivatives). Each
equation corresponding to an evaluation of the quartic outside the region
is replaced by an equation corresponding to a boundary condition. It is
clear from this construction that each boundary cell will require two
independent boundary relations, while cells removed from the boundary will
require a single relation.

The boundaries are assumed to be rigid. At the surface (the lower
boundary) a no-slip condition of zero velocity is invoked, since the fluid
is assumed to be viscous. This condition also applies to the perturbation
velocity, and implies that $w = w_z = r_i = 0$. At the upper boundary we

30

assume that the vertical velocity vanishes, and that there is no shear
stress or turbulent transfer across it. Applied to the perturbation
quantities this gives $w = w_{zz} = \eta_{zz} = \zeta_{zz} = 0$. We also assume for the
interim that $\rho = 0$ at $z = 0$. This set of boundary conditions is sufficient
for the differential equations (four conditions for the fourth order w
equation, and two conditions for each of the second order η and ζ equations).
The difference equations, however, are of fourth order in all quantities;
consequently, some non-physical boundary conditions are required to furnish
the additional constraints on the ζ and η equations.

Let us consider the w equations, where we have $w = w_z = 0$ at $z = 0$
and $w = w_{zz} = 0$ at $z = H$. At the cells adjacent to $z = 0$ and $z = H$ both
of the boundary conditions are applied at the positions of the boundary
one-half cell thickness away. In the cells one removed from $z = 0$ or
$z = H$ only one of the boundary conditions is needed; we choose the
condition $w = 0$ to be applied at the bottom and $w_{zz} = 0$ at the top. At
the lower boundary cell, for example, the equations derived from the
quartic consist of

$$f_3 = f_1 + \sum_1^4 a_j \, \Delta x^j \, 2^j \quad ,$$

$$f_2 = f_1 + \sum_1^4 a_j \, \Delta x^j \, 1^j \quad ,$$

$$f_0 = 0 = f_1 + \sum_1^4 a_j \, \Delta x^j \, (-1/2)^j \quad ,$$

$$f_0^1 = 0 = \sum_1^4 j a_j \, \Delta x^{j-1} \, (-1/2)^{j-1} \quad , \qquad \text{B-(20)}$$

where the first two equations correspond to evaluating the functions in

the mesh interior at $2\Delta x$ and Δx above the center of the boundary cell, the third equation corresponds to $w = 0$ at $-1/2\ \Delta x$, and the fourth corresponds to $w_z = 0$ at $-1/2\ \Delta x$. Equations B-(20) can be written in the matrix form B-(13)

(Bottom Boundary)

$$C = \begin{pmatrix} 1 & 1 & -1 & 3/4 & -1/2 \\ 1 & -1/2 & 1/4 & -1/8 & 1/16 \\ 1 & 0 & 0 & 0 & 0 \\ 1 & 1 & 1 & 1 & 1 \\ 1 & 2 & 4 & 8 & 16 \end{pmatrix} \begin{pmatrix} 1 & 0 & 0 & 0 & 0 \\ 0 & \Delta x & 0 & 0 & 0 \\ 0 & 0 & \frac{\Delta x^2}{2} & 0 & 0 \\ 0 & 0 & 0 & \frac{\Delta x^3}{6} & 0 \\ 0 & 0 & 0 & 0 & \frac{\Delta x^4}{24} \end{pmatrix} .$$

B-(21)

The remaining boundary matrices are obtained in a similar way. Suppressing the second matrix factor of C, which is the same for each case, we have

(Next-to-Bottom Boundary)

$$C = \begin{pmatrix} 1 & 1 & -3 & 6.75 & -13.5 \\ 1 & -1 & 1 & -1 & 1 \\ 1 & 0 & 0 & 0 & 0 \\ 1 & 1 & 1 & 1 & 1 \\ 1 & 2 & 4 & 8 & 16 \end{pmatrix} ,$$

B-(22)

(Top Boundary)

$$C = \begin{pmatrix} 1 & -2 & 4 & -8 & 16 \\ 1 & -1 & 1 & -1 & 1 \\ 1 & 0 & 0 & 0 & 0 \\ 1 & 1/2 & 1/4 & 1/8 & 1/16 \\ 1 & 0 & 2 & 3 & 3 \end{pmatrix} ,$$

B-(23)

(Next-to-Top Boundary)

$$C = \begin{pmatrix} 1 & -2 & 4 & -8 & 16 \\ 1 & -1 & 1 & -1 & 1 \\ 1 & 0 & 0 & 0 & 0 \\ 1 & 1 & 1 & 1 & 1 \\ 1 & 0 & 2 & 9 & 27 \end{pmatrix} .$$

B-(24)

In the calculations which have been carried out to date we have used these same matrices for the boundaries of the r-and o-submatrices, as well as for the w-submatrices. It will be desirable to reexamine the c boundary conditions and to relax the condition of $c = 0$ at the top boundary. In order to do so it will be necessary to define separate C-matrices at the boundaries for n, o and w. It is likely that the boundary conditions at the top of the mesh will not turn out to be very significant because the perturbation amplitudes should become small at high altitude. If the boundary is located high enough the solutions should not be affected by conditions there.

B.5   Numerical Solution of Matrix Eigenvalue Equation

We employ a standard subroutine package for solving the complex
eigenvalue problem. In order to place B-(9) in the form required by the
solver we multiply by the inverse of the B matrix

$$B^{-1}A\overline{X} = \omega\overline{X}$$ B-(25)

The B matrix inverse was obtained quite economically since it has a block
diagonal form

$$B = \begin{pmatrix} I & 0 & 0 \\ 0 & B_{22} & 0 \\ 0 & 0 & I \end{pmatrix} \quad \text{, where I is the identity matrix}$$

and the element B_{22} is purely imaginary. We form B_{22}^{-1} and construct

$$B^{-1} = \begin{pmatrix} I & 0 & 0 \\ 0 & B_{22}^{-1} & 0 \\ 0 & 0 & I \end{pmatrix} \quad .$$

The matrix $B^{-1}A$ is then submitted to the eigenvalue-eigenvector subroutine.

The computer solution of the complex general eigensystem was per-
formed with routines from the EISPACK (Smith, 1976) mathematics library. These are
FORTRAN-based routines published under the auspices of the Applied
Mathematics Division, Argonne National Laboratory.

The eigensystem package includes a driver routine "CG" which calls
a recommended sequence of subroutines to find the eigenvalues and (if re-
quested) eigenvectors of a complex general matrix.

The sequence of routines called is:

(a) CBAL: balances a complex general matrix.

(b) CORTH: given the balanced complex general matrix, reduces it to a sub-matrix of upper Hessenberg form by unitary similarity transformations.

(c) COMQR: (eigenvalues only) or COMQR2 (eigenvalues and eigenvectors): finds the eigenvalues and eigenvectors of the complex upper Hessenberg matrix using the QR algorithm of Francis (1961, 1962).

(d) CBABK2: forms the eigenvectors of the original complex general matrix by back-transforming those of the corresponding balanced matrix.

For convenience in comparing with test results the eigenvalues may be presented in two alternative formats; as real and imaginary parts of the eigenvector, or as the magnitude (amplitude) and phase of the eigenvector. Since each eigenvector contains an arbitrary complex amplitude, we have normalized the magnitude to 1 for presentation, and require the phase ϕ to be in the range $-\pi \leq \phi \leq \pi$. Examples of this presentation are given in subsequent sections.

Based on comparisons discussed in Section B-6, the computer code and eigenvalue subroutine are found to give quite accurate estimates of the lower mode eigenvalues. However, we have found that the $3I \times 3I$ element eigenvalue subroutine fails under a limited range of conditions. We believe that these conditions correspond to double roots of the indicial equation, which can arise under certain idealized conditions. This problem was encountered, for example, when $f = \bar{\sigma}_z = 0$. We have shown that under these circumstances the indicial equation becomes

$$(A_{11} - \omega I) (B_{22}^{-1} A_{22} - \omega I) (A_{33} - \omega I) = 0$$

35

where each of the quantities is an $I \times I$ matrix. For the cited case. $A_{11} = A_{33}$, and each of I eigenvalues is repeated. In this instance it is possible to reduce the order of the equations, for example by removing the equations for r, which are decoupled from the others. The resulting $2I \times 2I$ element problem is solved by the standard technique without difficulty. When parameters are chosen to correspond to a general problem the difficulty of eigenvalue degeneracy is not encountered. Consequently, it appears that the failure of the technique will be restricted to a limited range of parameters where a coefficient (such as f or $\bar{\rho}_z$) is very small, but not zero.

We anticipate that difficulty also might occur associated with a critical level (where $\omega = K \cdot \bar{U}$) but have not examined this point in detail (see Section D). It is expected that the amplitude of the perturbation will increase near the critical level, causing a breakdown of the equations. However, viscous damping will act to limit the growth; it is likely that a careful inclusion of absorption and choice of zoning will eliminate difficulties associated with critical layers.

B.6   Test Calculations

The computer code described in Sections B-1---B-5 above has been
programmed and tested against numerical solutions obtained with other
techniques and by other investigators. These comparisons verify that the
coding is substantially correct and that solutions are being obtained with
reasonable efficiency. Two classes of test problems were evaluated and com-
parisons were made.

In the first, the solutions of the inviscid negative buoyancy stability
problem were obtained. These can be compared with eigenvalues calculated
with the ZMODE iterative integration computer code, which we have employed
previously. When there is no wind these solutions correspond to internal wave
propagation with real eigenfrequencies. Using an analytic profile of buoyancy
and zero wind speed we calculate the eigenvalues as a function of wave number
using different numbers of zones in the vertical direction. We found that
the eigenvalues were all real, corresponding to undamped propagating internal
waves and that they occur in positive-negative pairs, corresponding to propaga-
tion in a given wavenumber direction and in a direction 180° from the first.
In these comparisons uniform zoning was used. For a case in which the buoyancy
frequency profile is given by

$$N^2 = C_1 \ X^4 \exp(-2X), \ 0 \leq Z \leq -75.,$$

where $Z =$ is the vertical height,

$$X = -Z/C_3 \text{ and } C_1 = 3.41 \ X \ 10^{-4}, \ C_3 = 25.0.$$

We have compared both eigenvalues and eigenfunctions. This case served as a verification that the matrix eigenvalue subroutines that we employ, after some initial difficulty, are calculating correct eigenfunctions. Using 20 zones we obtained the following eigenvalues for the case 'k' = 2.5cyc/km, (we compare them with the corresponding values resulting from the ZMODE computer code):

Mode	PERT	ZMODE
1	.00310	.00311
2	.00145	.00146
3	.00095	.00095
4	.00070	.00074

We also display the eigenfunctions corresponding to the vertical velocity perturbation w, as calculated by the two methods. In Fig. B-1 the eigenfunctions for mode 1 are shown; it was necessary to rotate the eigenfunction by an arbitrary phase and normalize it to unit maximum amplitude. Figs. B-2 and B-3 correspond to the second and third mode numbers. In each of these cases the phase of the eigenfunction is independent of altitude. These comparisons indicate that excellent agreement between PERT and ZMODE eigenvalues and eigenfunctions is achieved. Agreements for higher modes becomes less quantitative as the mode number approaches the number of vertical zones. It should be feasible, however, to form arbitrarily large mode number solutions by increasing the number of zones.

The second test problem corresponds to the instability of Ekman boundary layer flow. An idealized version of this problem was studied by Lilly (1965), who assumed that the atmosphere is neutrally stable and that the diffusivities are independent of altitude. The wind field is a solution of the

steady flow equations for a time-and altitude-independent geostrophic wind, and corresponds to the classical Ekman spiral.

$$\overline{U} = V_g (1-e^{-Z/D} \cos Z/D),$$

$$\overline{V} = V_g e^{-Z/D} \sin Z/D,$$

where V_g is the height-independent geostrophic wind, and $D = (\nu/\Omega)^{\frac{1}{2}}$ is the Ekman depth. Lilly calculated stability diagrams for the Orr-Sommerfeld equation and for a more general problem in which the Coriolis terms are included in the perturbation equations. Our test consisted in comparing with a large number of cases reported by Lilly. For the Orr-Sommerfeld problem, parameters close to the point of maximum instability were selected for several values of the Reynolds number $R = \dfrac{V_g D}{\nu}$, where V_g is the geostrophic wind speed, ν is the altitude-independent turbulent diffusivity, and D is the characteristic Ekman length (see Lilly, 1966 for a comprehensive discussion of this problem). In constrast to the internal wave problem, the eigenfunctions of the Ekman problem depend strongly on the direction, as well as the magnitude, of the wavenumber of the perturbation. We examined several cases in which the direction of the wavenumber vector, the Reynolds number, and the zoning were varied. In agreement with Lilly's results, we found that R = 65 is stable and that R = 110 and R = 500 are unstable. In both of the latter cases, instability is due to a single mode of the perturbation; all other modes are strongly damped. We also compared the real and imaginary parts of the eigen-frequency with Lilly's calculations (by inspection of his small diagrams). We found general agreement with the growth rate and phase speed of the dis-

turbance in the vicinity of maximum instability as well as at positions where the growth rate is smaller or negative. With few vertical zones (corresponding to the initial calculations) the eigenvalues did not compare as well as in the internal wave calculations. Increasing the number of uniform size zones improved agreement, but substantial differences (~ 25 in worst cases) still remained with 32 zones in the vertical. Modifing boundary conditions in zones one removed from the boundary (to relax the boundary constraint) restored agreement. Since the wind profile contains large shear near the surface, a nonuniformly zoned mesh was also tested. This produces some improvement, but we have not had the time to determine optimum mesh parameters or the enhancement of accuracy. Subsequently, the Coriolis terms were added to the matrix equations and a test of the complete system of equations was made. We calculated several cases recorded by Lilly corresponding to the wavenumbers where the inviscid and the parallel instabilities have maximum values. In addition to the eigenvalues we were able to compare our eigenfunctions with those given by Lilly. For a Reynolds number of $R = 110$ the local maximum value of instability due to the parallel mode is located near $k = 0.3$ and $\varepsilon = -11^{\circ}$. For these values of the parameters we obtain $\omega_R = .124$, $\omega_I = .0052$, which are in good agreement with Lilly. In order to compare eigenfunctions we formed the absolute value of the normalized amplitude and the phase of the eigenfunctions. In Fig. B-4 we show these quantities for the w eigenfunction; they are in good agreement with Lilly. The inviscid mode has its maximum near $|k| = 0.5$, $\varepsilon = 8^{\circ}$; the corresponding eigenvalues are $\omega_R = .0461$, $\omega_I = .0021$, and the eigenfunctions are shown in Fig B-5. As indicated by Lilly, the Coriolis terms modify the stability of the boundary layer significantly through the parallel instablity mechanism. The effect

of these terms is to lower the critical Reynolds number and to change the character of the unstable motion. Consequently, it is important to include these terms in the stability analyses of a neutrally stable boundary layer even though at first consideration one would anticipate that the Coriolis terms are too small to affect the results.

It should be remarked in passing that the above formulation does not include all of the terms containing the Coriolis parameter. Referring to (8) we find that the perturbation equations for τ and w have terms proportional to (U_g, V_g) and f which we discuss below.

On the basis of the above comparisons it is now quite likely that the major terms of the perturbation computer codes are correct, and that the numerical methods developed for its solution are working satisfactorily. There remain, however, a large number of terms which have not been tested. These include terms involving gradients of diffusivity, vertical mean velocity, and geostrophic terms in the perturbation equations. It will be necessary to test these terms as well in the course of performing a comprehensive study of boundary layer instability.

A difficulty arises in trying to explore the many parameters which the computer code contains. Ultimately these free parameters will be constrained by the realizability of the mean flow solution. That is, it is not practical or realistic to independently vary the many degrees of freedon presented by the mean flow quantities, since they must be related to each other in such a way that they represent a consistent solution of the mean boundary layer equations (as, for example, in SIGMET). This consideration, in fact, constrained our formulation, dictating several features of PERT, such as the matrix form and the non-uniform zoning. Several calculations have been performed in this mode,

41

and they are reported in Section B-7. However, chronologically we first carried out some calculations designed to show the capabilities of PERT by obtaining new boundary layer stability results. These findings are also reported in the next section.

B-7   Stability of Boundary Layer Flow

In the previous section tests of the PERT computer code were described
for two classes of problems differing greatly in physical content; wave
propagation in a stably stratified medium, and secondary circulation of an
idealized shear flow in a neutrally stratified atmosphere. These problems
show that the technique gives expected results in these cases, so that we may
now look at several more general boundary layer problems. In this section the
results of calculations sampling some of the additional parameters which affect
boundary layer stability are reported. The combined effects of shear and
stratification appear not to have been investigated. First we explore the
effect of a constant density gradient added to the Ekman flow problem invest-
igated in Section B-6. The mean wind configuration of the Lilly study is retained,
the diffusivities are equal and independent of altitude as before, and the
density gradient is taken to be independent of altitude as well. We will
explore how the Orr-Sommerfeld stability diagrams are modified by this constant
density gradient; we expect to find increased instability when the atmosphere
is positively buoyant, and stabilization of the shear instability for sufficiently
large stable stratification. The density gradient introduced into the perturba-
tion equations is a dimensionless quantity scaled by the Ekman layer depth,
D, employed in the neutrally stable case. The figures and discussion below
refer to this scaled quantity $\rho_z{}^* = \dfrac{\bar{\rho}_z \, D}{\bar{\rho}}$. A typical value of the potential
density gradient in the atmosphere of 10^{-5} m^{-1} gives a scaled density
gradient $\simeq 3 \times 10^{-3}$.

For the case of the Orr-Sommerfeld equation with R = 110 we have
explored the dependence of the growth rate on the density gradient, $\rho_z{}^*$.
Using $K_x = 0$, $K_y = 0.5$ (near the point of maximum instability of the neutrally
stratified case), we varied the density gradient as shown in Fig. B-6.

43

A very small stable density gradient is sufficient to achieve stability ($\rho_z{}^* \simeq -.0002$); more strongly stable atmospheres exhibit damping for all modes of the perturbation. It is interesting, however, that the growth rate does not continue to decrease in the stable region because another mode assumes the role of the largest imaginary eigenvalue. This mode becomes dominant at $c_z{}^* \simeq -.0004$, and its magnitude decreases slowly for more stable stratification. This mode (and other modes having about the same damping rate) is probably an internal wave mode, which becomes more prominant as the Brunt-Vaisala frequency is increased. The dependence of the growth rate on the magnitude and direction of the wavenumber at $\rho_z{}^* \simeq -.0001$ for $R = 110$ is shown in Fig. B-7. This shows that the configuration of the unstable region is not substantially changed, but, as expected, the extent of the unstable region is decreased.

The character of the solution also changes rapidly when the density gradient becomes positive. In Fig. B-6 another mode becomes most unstable when $\rho_z{}^* \simeq .0002$. For this mode the growth rate is a rapidly increasing function of $\rho_z{}^*$. For typical values of unstable atmospheric stratification the predominant mode will be this convectively unstable one; the shear instability will not influence the solution appreciably. It appears from a couple of calculations that the convective mode is very much less directional than the shear mode.

We have also performed calculations for the Orr-Sommerfeld problem with $R = 500$, for which the unstable region in K_x, K_y space is larger. In this case, as indicated in Fig. B-8, the density gradient must be more negative ($c_z{}^* \simeq -.0015$) to overcome the shear instability. As in the lower Reynolds number case, there is a crossing of mode trajectories. The damping rate for the most nearly unstable mode in the larger gradient region is now quite small, corresponding to the larger Brunt-Vaisala frequency.

In view of the observed effect of the Coriolis force on the Ekman stability criterion, we have repeated several of the calculations assessing the effects of stratification with the Coriolis terms included. First, we examine the effect of the same terms retained by Lilly and included in our Coriolis test calculations (see Section B-6). The effect of density gradient on growth rate for this case is shown in Fig. B-9. As expected from Lilly's diagrams the instability near $\rho_z^* = 0$ is decreased for $\cdot = 0.5$, $\epsilon = 0$. However, for stable stratification the "gravity wave" mode, which soon dominates the stability diagram, shows very little dependence on the Coriolis parameter. Consequently for ρ_z^* larger than that for mode crossover, the most unstable mode growth rate approaches that with $f = 0$. Similarly, for unstable stratification the "convective" modes are not dependent on f so that sufficient instability also reduces the influence of the Coriolis paramiter. These properties are displayed in Fig. B-9, by comparison with Fig. B-6 (with $f = 0$). It is interesting that the mode responsible for instability at $\rho_z^* = 0$ shows markedly smaller growth rate with the Coriolis term present over the full range of density gradient.

The effect of the large-scale convergence/divergence of the mean flow field also modifies atmospheric stability. We have explored this effect by adding the terms in $\overline{W}$ and D to the neutral Ekman boundary layer perturbation equations. Starting from the Lilly formulation in which the standard Coriolis terms are included, we added a height-independent divergence term D (which may be either positive or negative). The corresponding mean vertical velocity is linear with height z,

$$\overline{W} = - Dz.$$

45

Starting from the case R = 110, κ_x = 0, κ_y = 0.5, we have varied D to assess
its effect on the growth rate of the most unstable eigenvalue. In Fig. B-10
the growth rate is a function of the scaled divergence in a range of values
actually found in the atmosphere. We find that the growth rate is quite
insensitive throughout this range of convergence and divergence. It should
be remarked that the effect of moisture condenation is not taken into account
in this investigation; the effect of lifting condensation on convective instability
will be much larger.

Finally, we have performed several calculations using the capability to
transfer data from the SIGMET code to the PERT code. In this procedure all
of the mean variable profiles needed to initiate the linear perturbation
calculation result from the unperturbed boundary layer calculation. Data are
extracted from a particular time of a time-dependent calculation, even though
this is not entirely consistant with the time-independent perturbation for-
mulation. However, the SIGMET solution over a water surface is slowly changing.
These calculations differ primarily from previous calculations in having
profiles of mean variables which are not simplified for the sake of convenience.
The wind field can change in magnitude and direction, the buoyancy field may
contain simultaneously megative and positive regions, and the turbulent transfer
coefficients may vary with altitude as required by the boundary layer equations.

Several mathematical difficulties prevented us from carrying out these
calculations until very date in the investigation. Consequently, we have not
been able to explore the many parameters governing this boundary layer stability
problem. We are restricted to sampling the stability diagrams for a single case.

The SIGMET problem has been reported in Section A; it corresponds to cycle
72 (time = 1608 local time) of a marine summer boundary layer having a

geostrophic wind speed of 10 m s. Some of the profile data are shown in Figs. A-1 and A-2. We repeated the calculation with lower resolution using 20 zones in order to reduce the computational expense of the PEFT calculations. Subsequently, a survey was made of linear stability as a function of wavenumber. The dispersion diagram for these calculations is shown in Fig. B-11. A number of the modes appear to be internal waves displaced by the geostrophic wind speed. The up-wind traveling waves are more complicated, displaying several mode crossings. These later waves will encounter critical levels at lower altitudes of the boundary layer. Apparently, a shear-unstable mode is also present. The magnitude of the growth rate of this mode increases with wavenumber as shown in Fig. B-12. The similarity of the dispersion diagram with that from the internal wave study of Section D is quite striking. Further investigation of this an similar problems is warrented.

B.8   Summary and Remarks

The linear stability of boundary layer flow has been investigated under quite general conditions of wind shear, stratification and turbulent exchange. Perturbation equations have been derived admitting arbitrary dependence of mean flow quantities on altitude, and these are formulated for numerical solution as a matrix eigenvalue problem. A computer program (PERT) containing this formulation have been developed to evaluate quite general boundary layer stability problems. Calculations have been performed duplicating known results for internal wave propagation and Ekman flow instability. The stability of generalized Ekman flow in stratified atmospheres has also been studied. We have determined the amount of negative buoyancy needed to stabilize the shear instability and have displayed some of the systematic features of the stability diagram. An advantage of the matrix method is that all of the lowest modes of the eigenvalue problem are obtained. Using the resulting data it then becomes possible to trace the competition of several modes. For the problem of a stratified shear boundary layer we found that the crossing of different mode trajectories is responsible for the changes in stability character when stratification departs from neutral in both the positive and the negative direction. In the case studied we found that only the mode responsible for instability near neutral stratification is sensitive to the Coriolis term.

We have also investigated the effect of the large-scale convergence or divergence of the horizontal wind field on stability. This field is almost always present due to synoptic weather features such as cyclones and anticyclones. When this term and the resulting mean vertical velocity were

added to the neutrally stable Ekman boundary layer we found that the growth rate of instability was modified, but that within the range of realistic values of convergence or divergence the magnitude was not appreciably changed. We conclude that its effect on secondary circulations not involving moist processes (which have not been included) is minimal.

A version of the PERT computer code has been developed which accepts data from the one-dimensional boundary layer computer code, SIGMET. To demonstrate this capability a linear stability analysis of a case involving a marine atmosphere has been performed. The selected case contains stratification which is slightly stable through the mixing layer and quite stable above. Rather small turbulent intensity is present in the lower layer. Several modes may be identified as corresponding to damped internal waves. One mode of the eigenvalue spectrum displays exponential growth; this presumably corresponds to the shear layer instability (without Coriolis effect, since this term is currently omitted from the version of PERT used in this calculation).

In Section D some additional PERT calculations are presented in connection with an investigation of the internal wave spectrum to be expected in a marine atmosphere.

To date, we have been able to indicate qualitatively the range of capabilities of the linear stability analysis through the illustrative calculations described above. Due to limitations of funds and time we have not been able to exploit this tool to its full capability. In assessing our progress toward understanding instability and secondary circulations of marine atmospheres it is important to place linear analysis in perspective.

The advantages of this approach are quite significant. As we have shown, essentially all physical effects can be taken into account, and the resulting calculations make quite modest demands in terms of computer time. With this method it is feasible to carry out hundreds of separate calculations, thereby surveying the stability parameter space more thoroughly than possible by other methods. The accuracy of the linear perturbation approach is more difficult to evaluate, since it depends on the particular response of the system. To illustrate, the internal wave solutions are either undamped or slightly damped by viscosity. They will frequently have small enough amplitude to satisfy the linear approximation. Under certain conditions, however, they will grow in amplitude until they can no longer be considered to be of small amplitude; they then modify the "unperturbed" solution and are no longer governed accurately by the linear equations. When there exists an unstable mode we expect that the linear solution ultimately will break down. In that event the linear equations suggest the conditions for the onset of instability but give no information on the asymptotic state (if one exists) of the secondary circulation. Clearly, there is no substitute for a nonlinear calculation if one requires information about the state that the system reaches at late time. Information about linear and nonlinear behavior appears to be complementary in many respects.

Our linear perturbation studies should be augmented with nonlinear calculations, as proposed earlier. But it will also be desirable to extend the linear calculations in several respects. We are currently improving the accuracy of the PERT code by introducing double precision arithmetic in selected parts of the code. There is also potential improvement for more

careful boundary conditions and zoning. From the physical point of view further work is needed on time-dependent unperturbed solutions, on compressibility, and on moisture effects. Additional work on coupling with the boundary layer codes will enhance our ability to investigate realistic problems in convective instability. Finally, as mentioned earlier, we believe that the applications of the PERT code are far from exploited. Considerable information can be obtained about the systematics of stability/instability of marine boundary layers. Not the least of the benefit will come from enhanced understanding of the dynamics of competing modes.
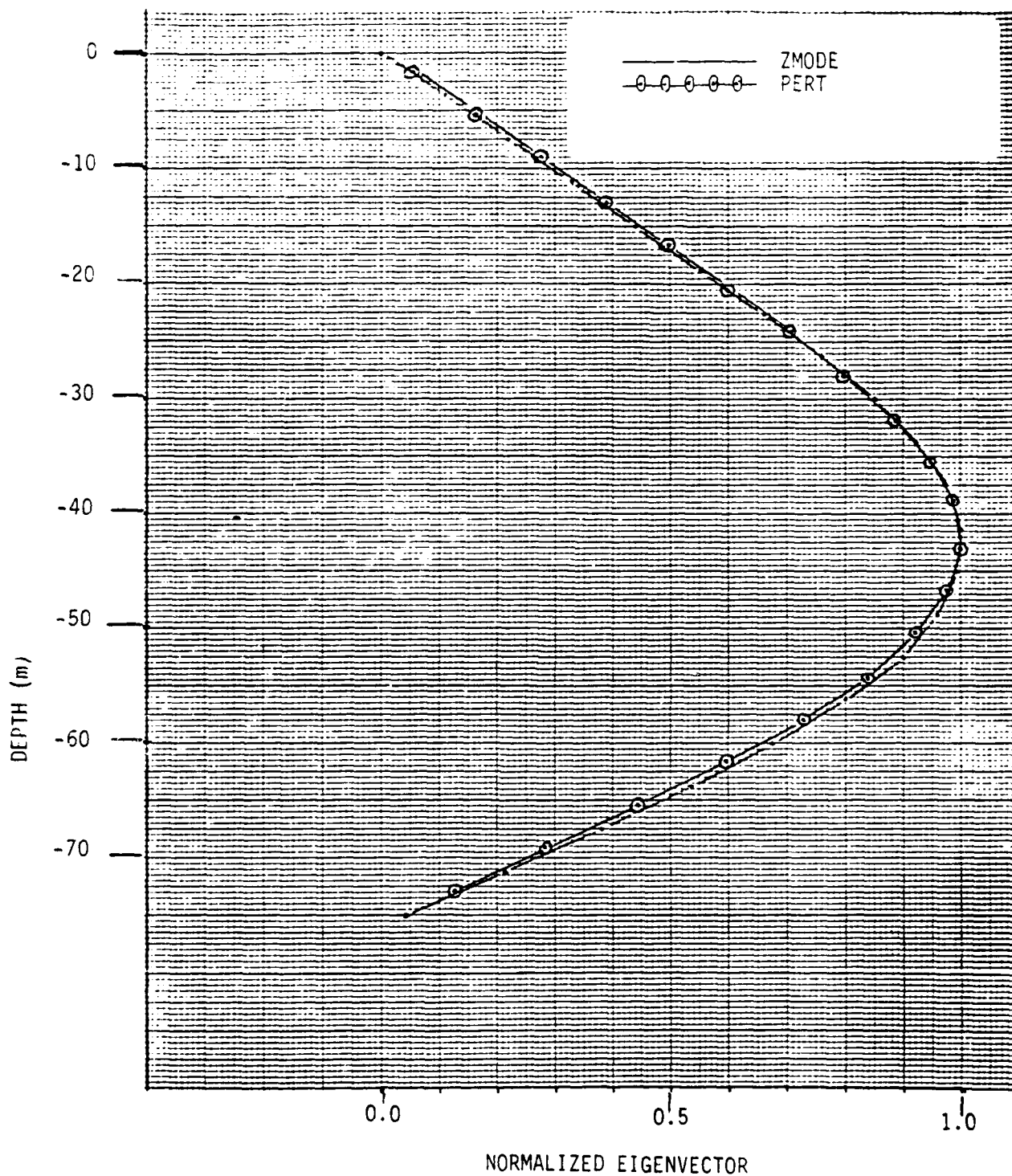
FIGURE B-1. Comparison of Mode 1 eigenfunctions for PERT and ZMODE internal wave calculations, $|k|$ = 2.5 cyc/km.
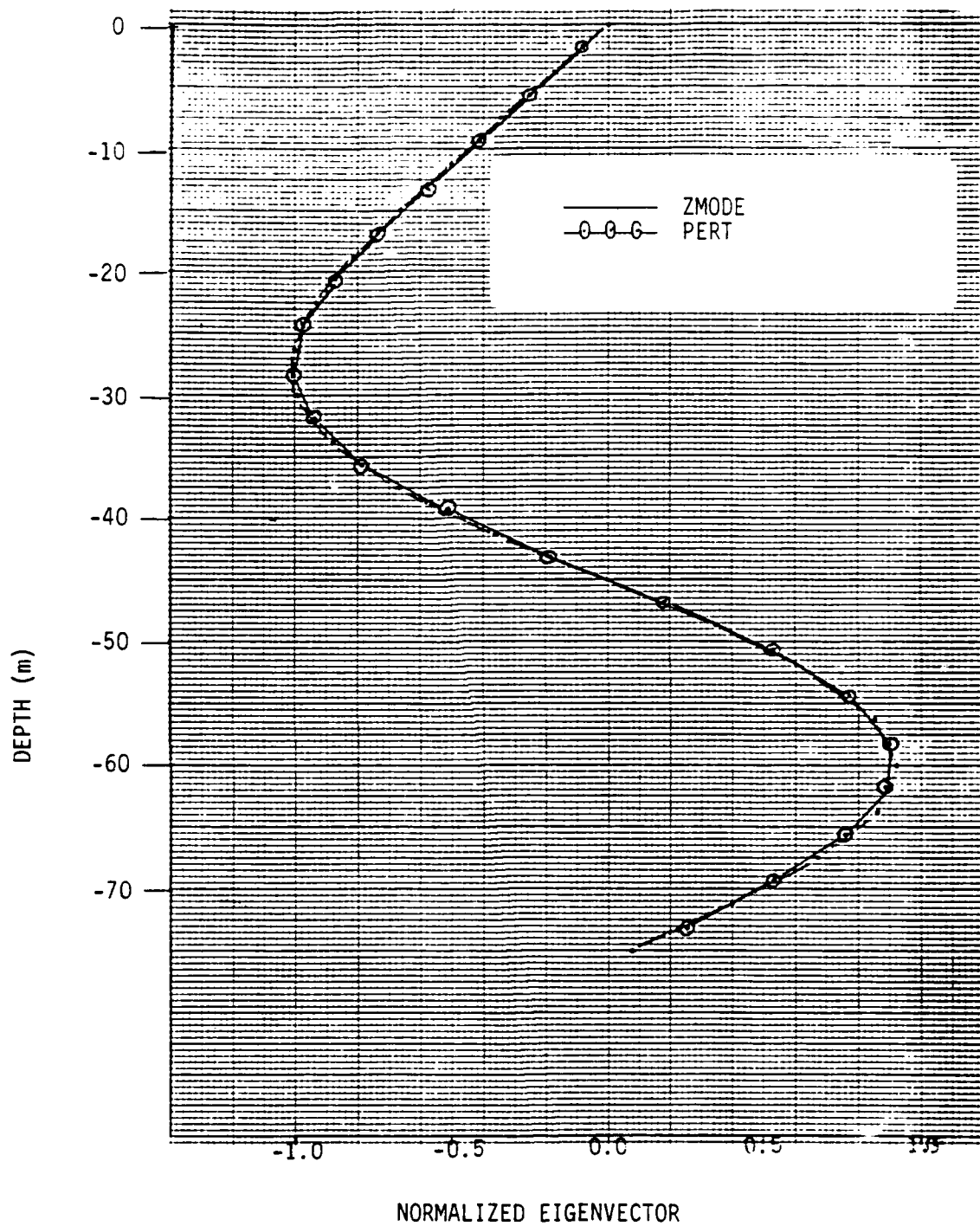
FIGURE B-2. Comparison of Mode 2 eigenfunctions for PERT and ZMODE internal wave calculations, |k| = 2.5 cyc/km.
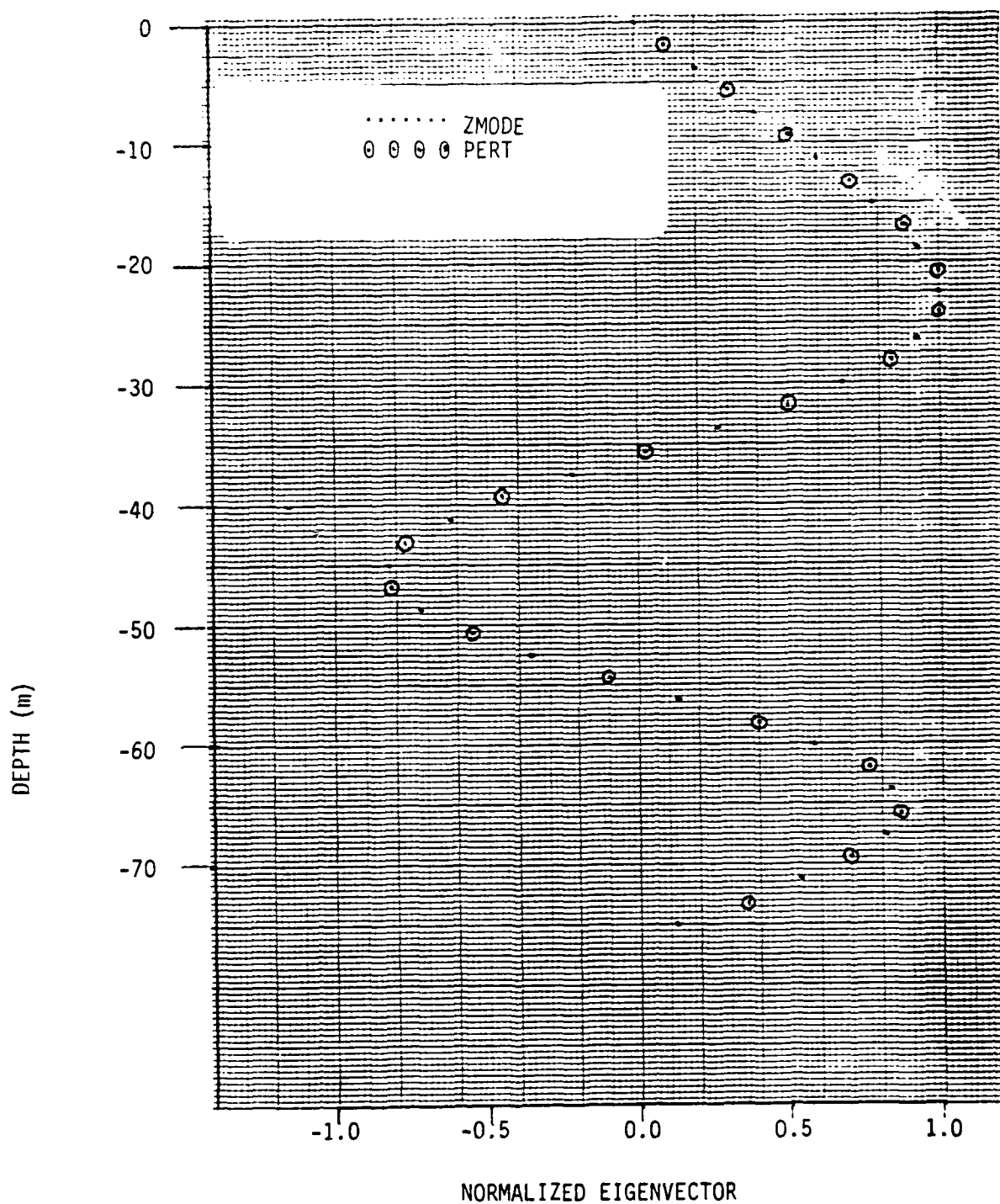
FIGURE B-3. Comparison of Mode 3 eigenfunctions for PERT and ZMODE internal
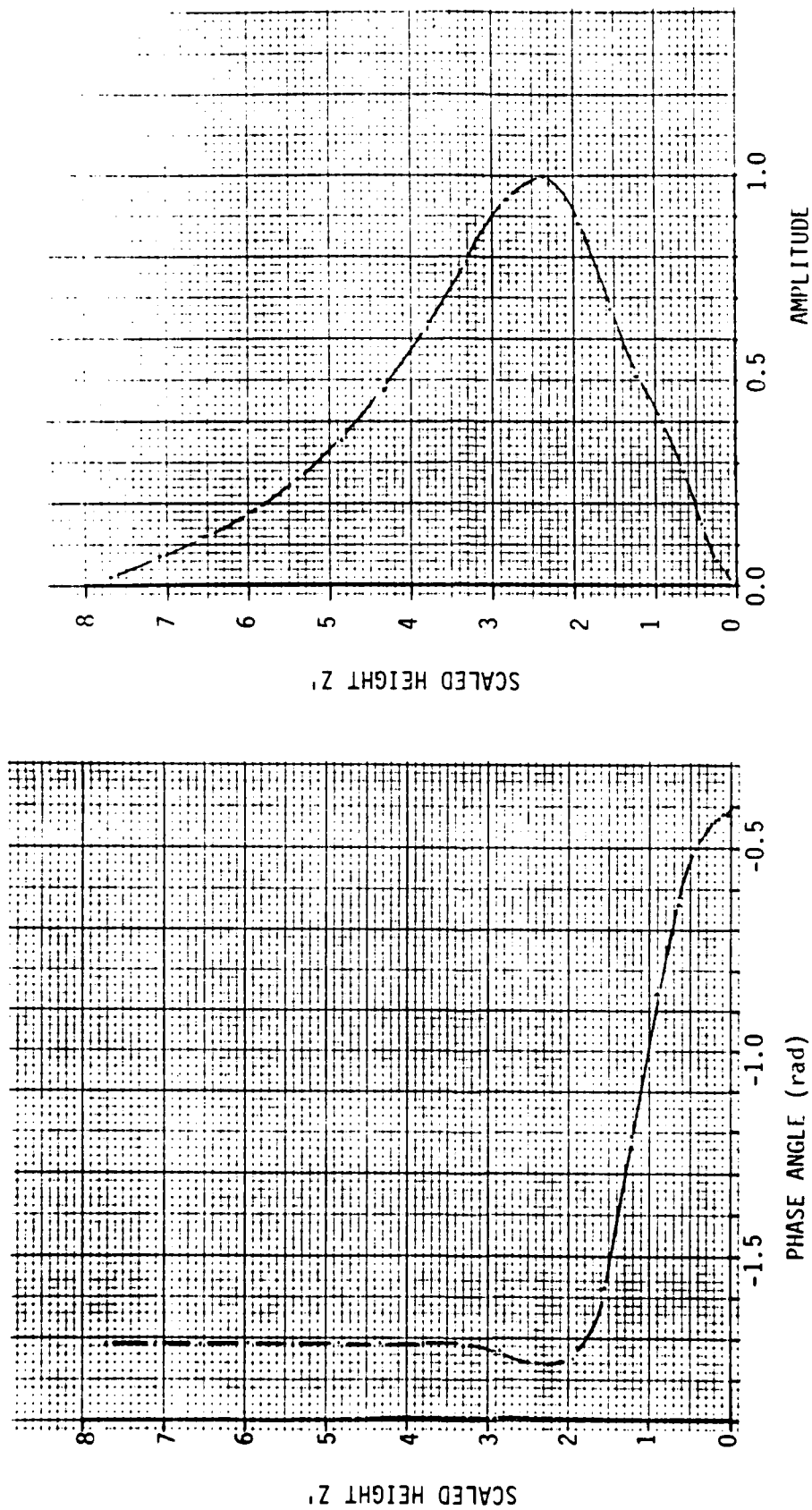wave calculations, $|k| = 2.5$ cyc/km.
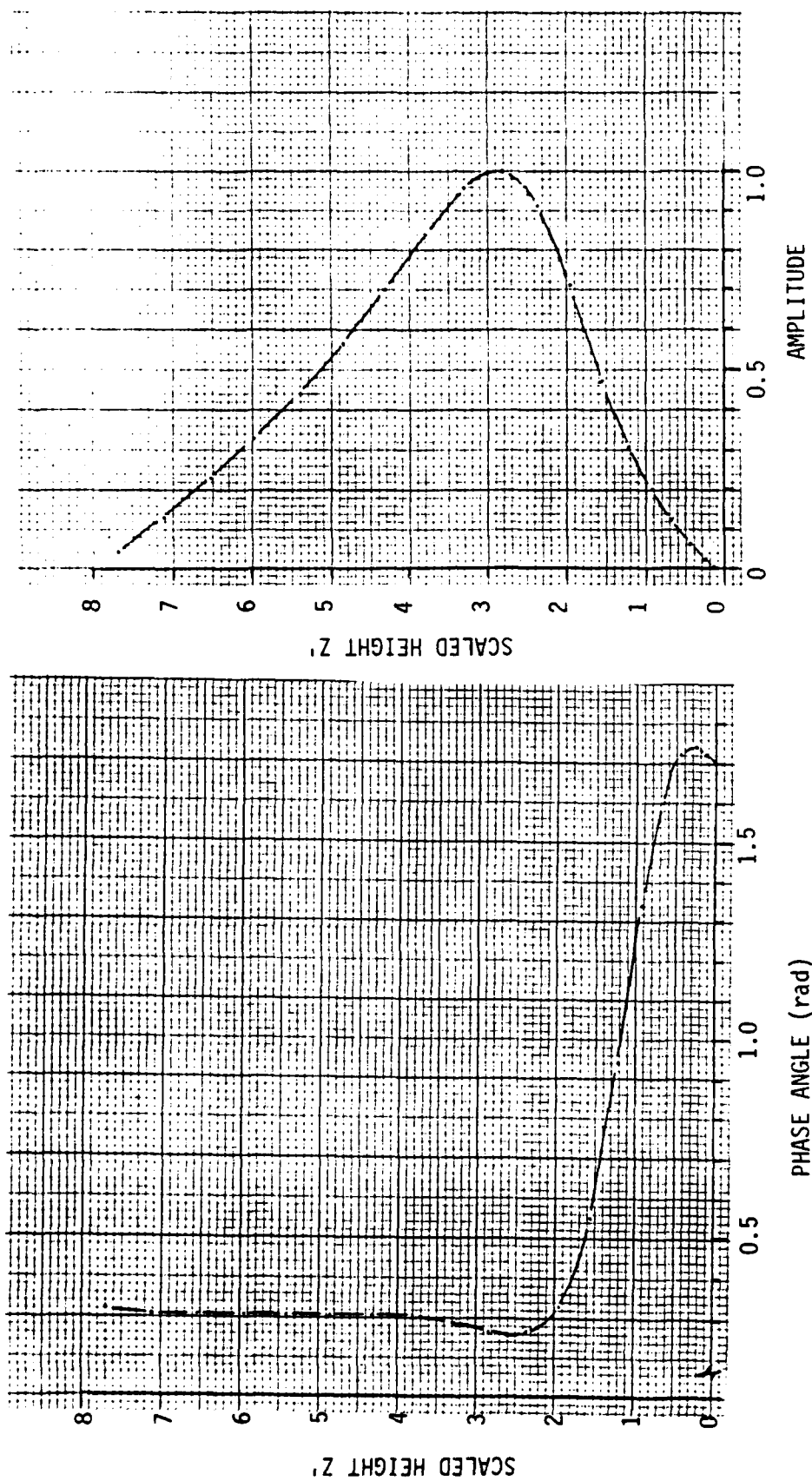
FIGURE B-4 Amplitude and phase angle of the vertical velocity for the most unstable mode for the Ekman shear instability problem. R=110.0, |k|=0.3, ε=-11°.

55

FIGURE B-5. Amplitude and phase angle of the vertical velocity for the most unstable mode for the Ekman shear instability problem. R=110.0, $|k|$=0.5, ϵ= 8^0.
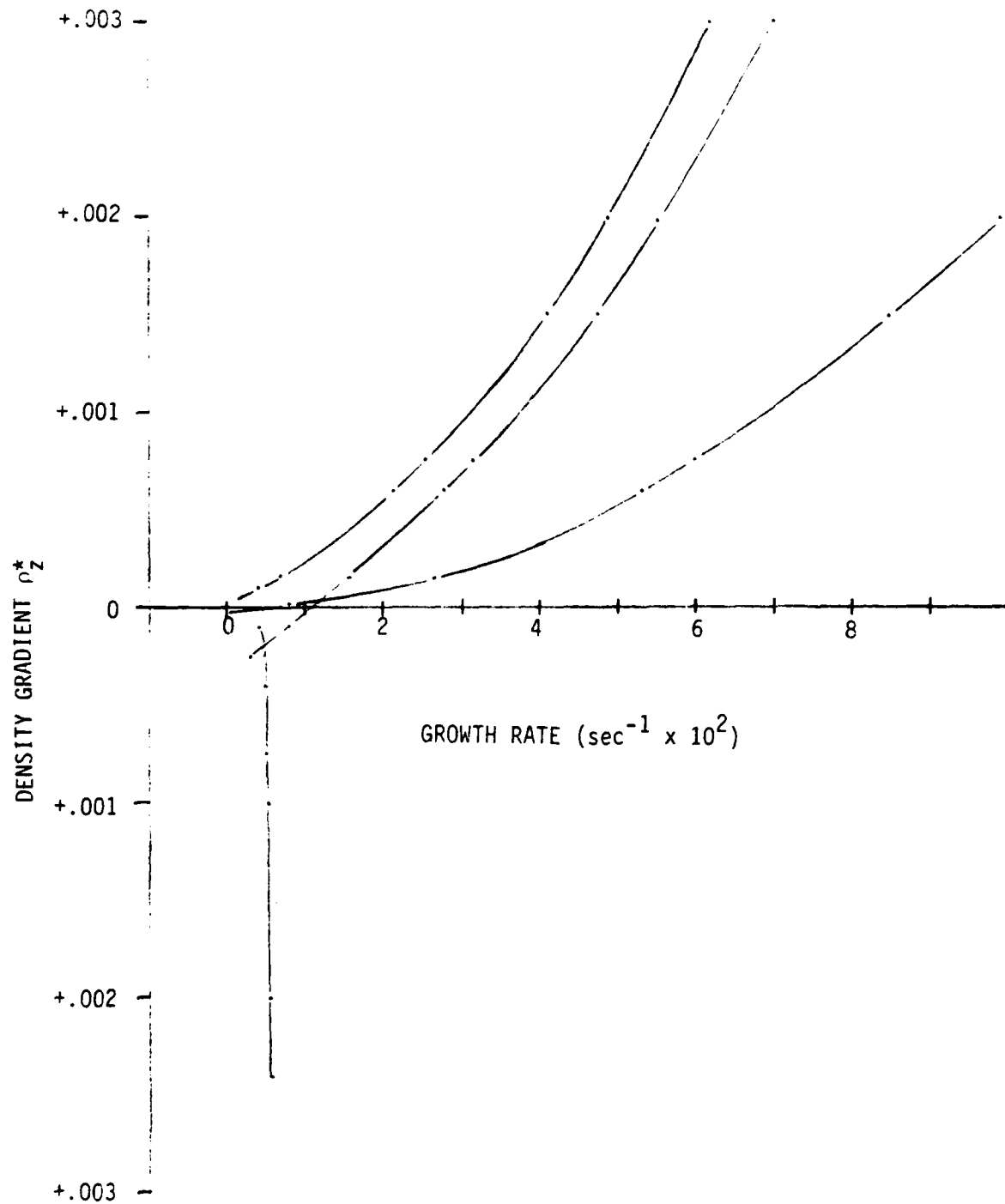
56
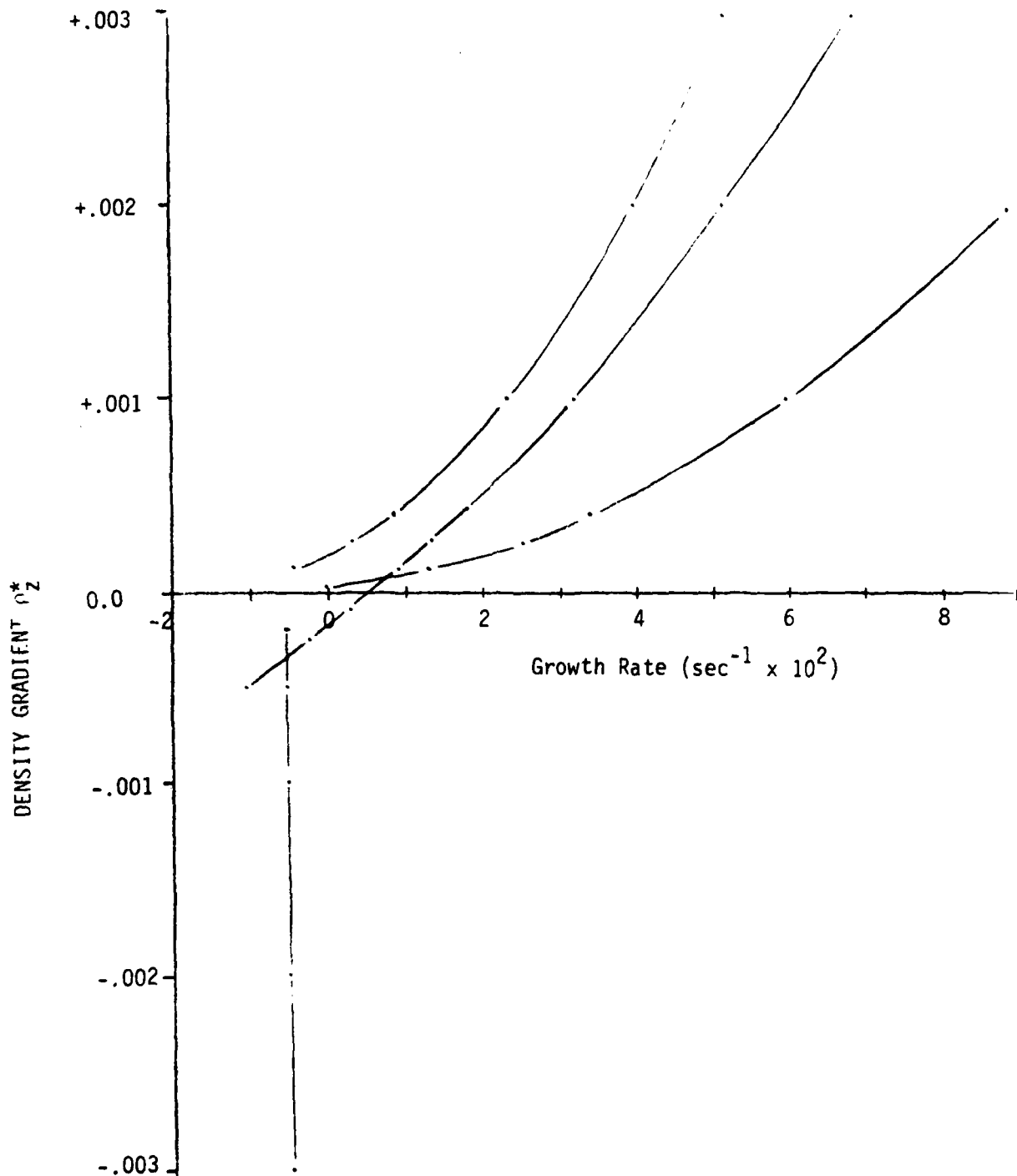
FIGURE B-6. Growth rate of most unstable modes as a function of normalized density gradient ρ_z^* for the generalized Ekman shear instability problem. $R=110.0$, $^z|k|=0.5$, $\varepsilon=0^\circ$.
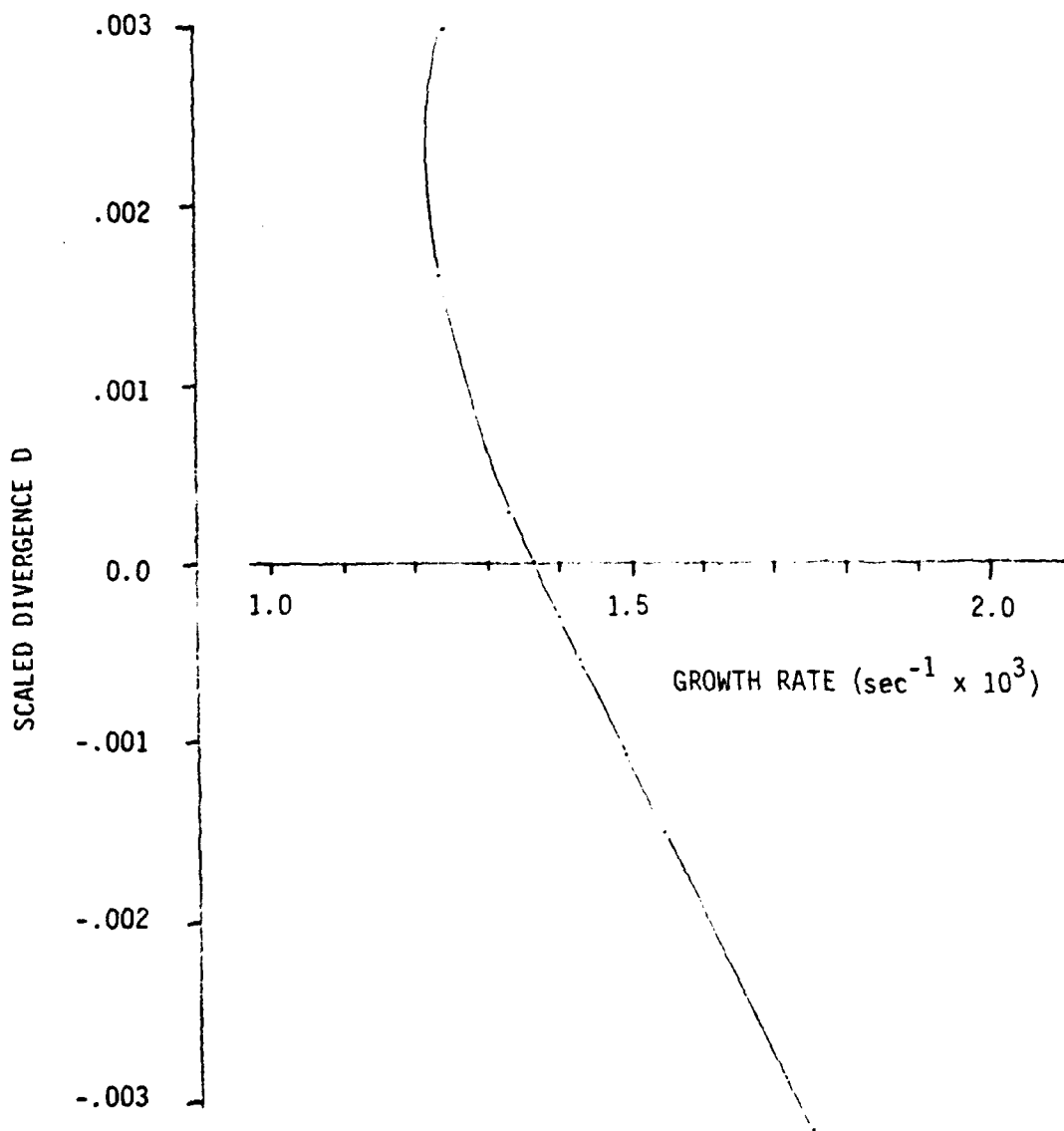
MAGNITUDE

$k = 0.4$

$k = 0.5$

$k = 0.6$

+.0022

+.0023

+.0016

-.0013

+.0013

+.0031

+.0025

+.0040

+.0033

+.0040

+.0033

-10°

-5°

0°

5°

10°
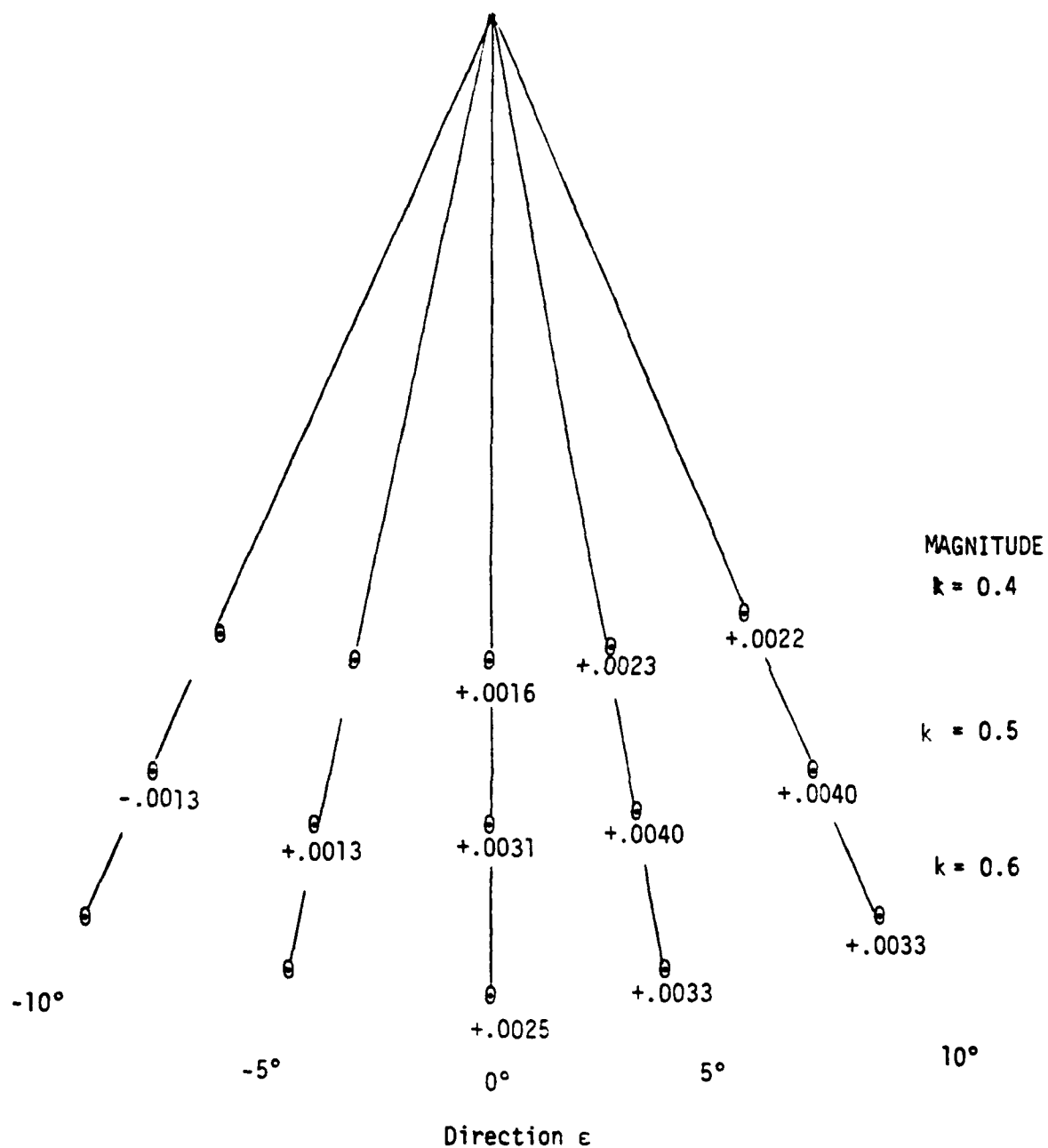
Direction ε

FIGURE B-7. Growth rate of most unstable mode as a function of wavenumber magnitude and direction for the generalized Ekman shear instability problem.   R=110.0, ε_z^*=-0.0001.

58

FIGURE B-8. Growth rate of most unstable modes as a function of normalized density gradient $\rho_z^\star$ for the generalized Ekman shear instability problem. $R=500.0$, $|k|=0.5$, $\varepsilon=20^0$.

FIGURE B-9. Growth rate of most unstable modes as a function of normalized density gradient ρ_z^* for the generalized Ekman shear instability problem with Coriolis terms included. $R=110.0$, $|k|=0.5$, $\epsilon=0°$.

FIGURE B-10. Growth rate of most unstable modes as a function of scaled divergence for the Ekman shear instability problem with coriolis terms included. R=110.0, |k|=0.5, $\varepsilon=0^8$.
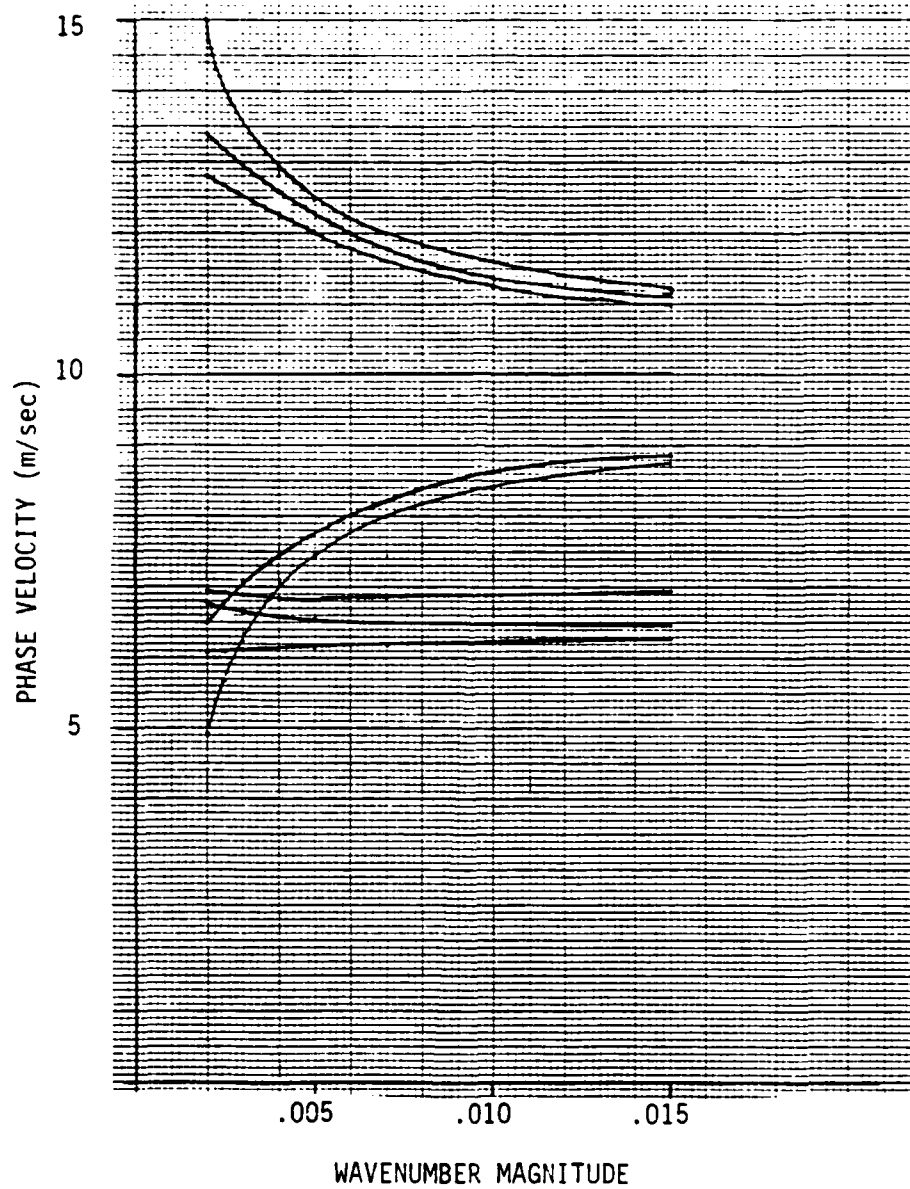
FIGURE B-11. Phase velocity as a function of wavenumber magnitude for various modes corresponding to SIGMET-calculated atmospheric parameters $\_=0^8$.
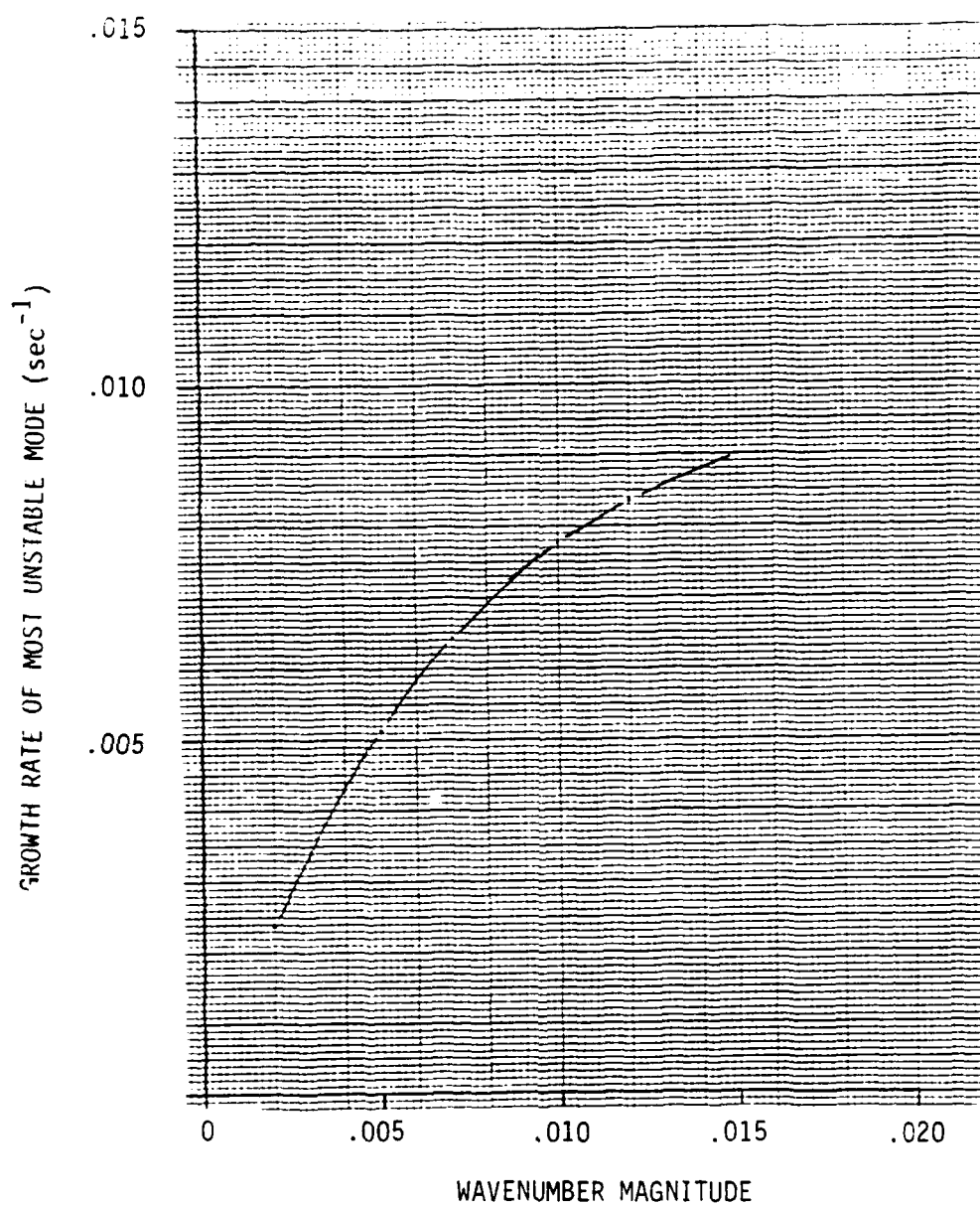
FIGURE B-12. Growth rate of most unstable mode as a function of wavenumber magnitude corresponding to SIGMET-calculated atmospheric parameters. $\varepsilon = 0^0$.

C.   Radar Properties of the Marine Atmosphere

An apparent correlation exists between a surface radar duct and certain convective phenomena. Consequently, it is desirable to try to bring convective instability of the marine boundary layer into the same theoretical framework as that of tropospheric ducting. It is also desirable to estimate the crossection for radar scattering from the marine atmosphere. Calculations with the SIGMET 1-D boundary layer computer code were described in the final report of the first phase of this work (Freeman, 1979). At that time we incorporated a calculation of the radar structure function based on the variances and covariance of temperature and water vapor fluctuations into SIGMET. Consequently, we were able to associate profiles of the radar structure function with various environmental conditions governing the marine atmosphere. An example of this data is shown in Fig C-1, taken from the SIGMET calculation described in Section A. The radar structure function is large at the base of the temperature inversion and in a zone adjacent to the surface.

The latter region under appropriate circumstances can result in a surface radar duct through channeling of the beam by the gradient of refractivity. A quantity which measures the ability of the atmosphere to support an over-the-horizon radar duct is the height-modified microwave index of refraction

$$M = n-1 + \frac{Z}{R},$$

where Z is the altitude, and R is the radius of the earth. This quantity depends on the index of refraction, n, which is a function of pressure

64

p, temperature T, and humidity C:

$$n - 1 = \frac{a}{T} P(1 + \frac{bc}{T}) \quad .$$

A negative gradient of the quantity M indicates that ducting will occur. Consequently, the altitude range through which the gradient is negative determines the depth of the surface duct. In Fig. C-2 we show the profile of M early in the SIGMET calculation mentioned above. This indicates that a surface duct is present having a height of ~15m, in addition to an elevated duct at abound 500m. The M-profile later in the calculation (Fig. C-3) at local time = 0108., shows that the surface duct has essentially dissipated while the elevated duct has risen in altitude.

Recently, several calculations of the evolution of profiles of microwave refractive index have been presented by Burk (1980a), who also employs a 1-D boundary layer model. Several different cases are examined, two of which correspond to marine atmospheres. These cases display surface duct formation, although greater attention is devoted to elevated ducts. The characteristics of the surface ducts are not resolved in the figures presented by Burk and he has not studied the systematics of these ducts.

We have not had an opportunity to survey the dependence of duct height on atmosphere parameters either. However, it is clear that such a study is feasible using a tool like SIGMET. In addition to extending our understanding of conditions under which ducting takes place, it could be determined to what degree the surface duct is associated with the susceptability of the atmosphere to trigging of convection.

A somewhat similar study can be made of the radar structure function.

Again, Burk (1980b) has recently given examples of the profiles of the
microwave structure function, in addition to those for the optical range
and for acoustics. Using the same three cases for illustration as in
Burk (1980a), the altitude dependence and relative contributions of temp-
erature and moisture fluctuations were evaluated. Calculations have also
been made recently (Burk, 1980c) examining the effects of a gradient of
sea surface temperature on radar ducting and the structure coefficient.
These calculations indicate that there is a substantial change in these
quantities due to air advection over moderate gradients. Such effects
are expected to be significant in coastal waters. Similar calculations
were performed by Lewellen and Teske (1975).

We can conclude (as in the case of ducting) that theoretical
models of boundary layer structure and associated radar structure function
are available. The models have not been carefully compared with data or
evaluated parametrically. Investigations of the systematics of ducting
and scattering are desirable as part of a program to improve understanding
of the radar properties of the marine atmosphere. In particular, radar
properties can be correlated with weather conditions affecting other local
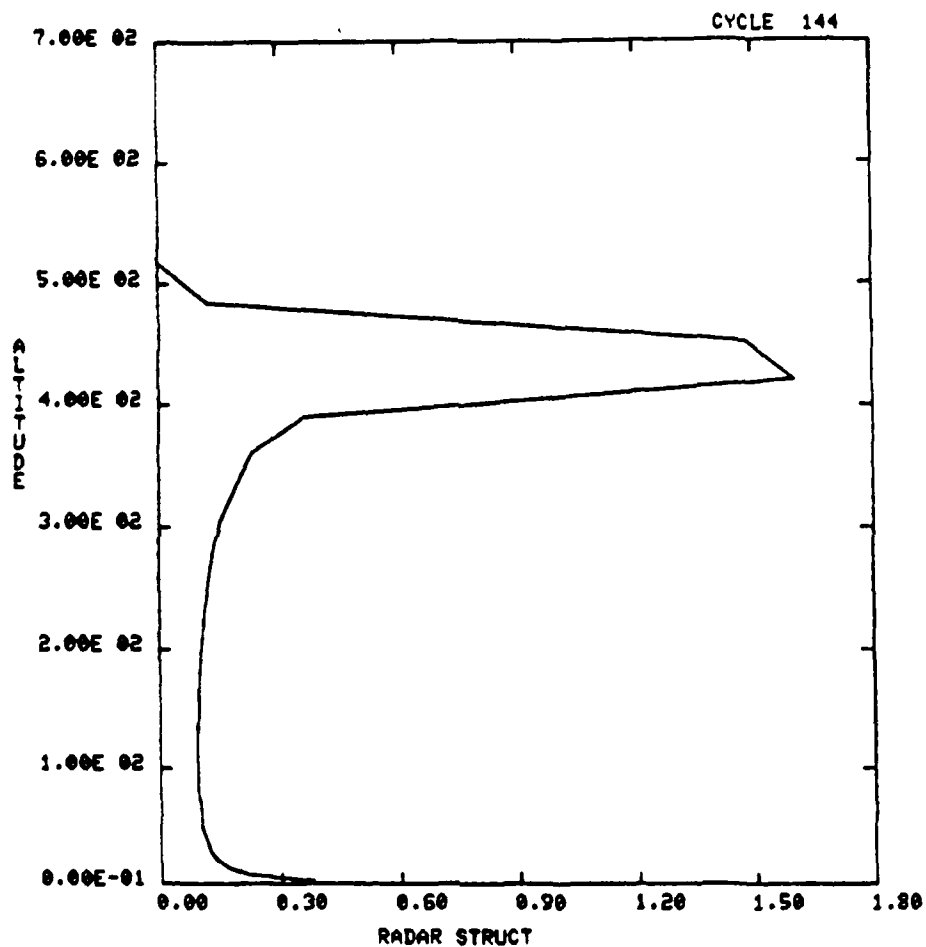phenomena such as the formation of convective cells.

FIGURE C-1. Radar structure function as a function of altitude corresponding to SIGMET-calculated atmospheric parameters. Local Time =0108 hours.
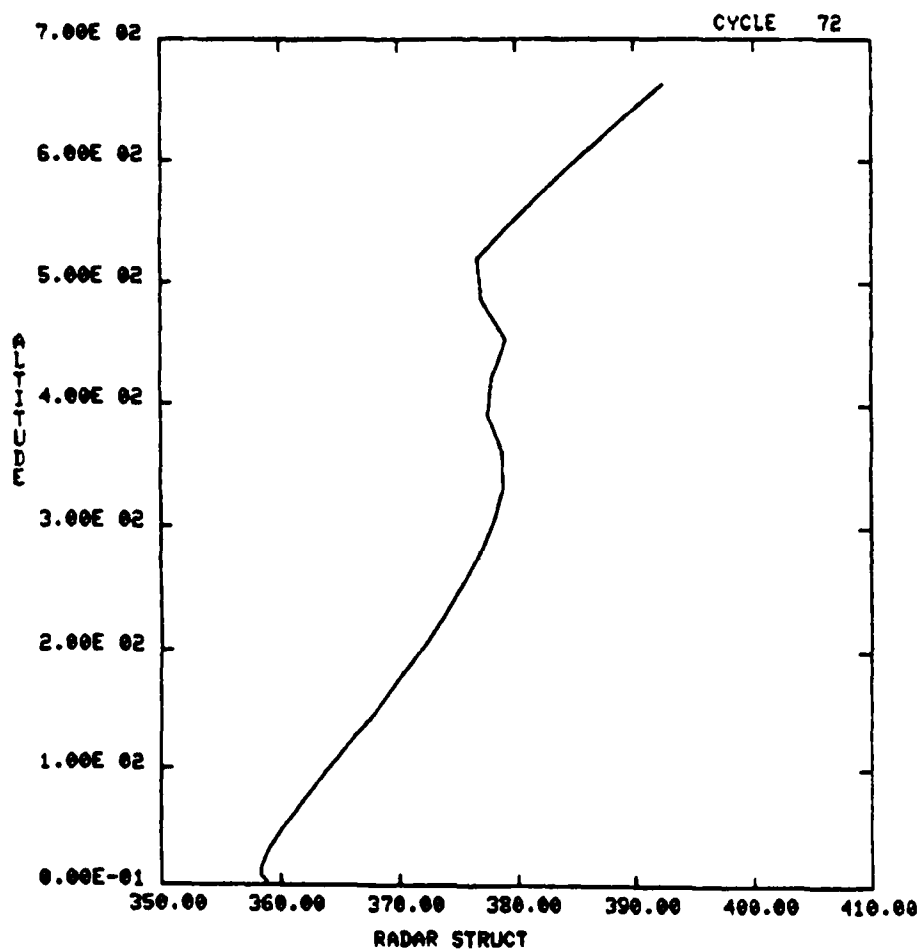
FIGURE C-2. Modified radar index of refraction as a function of altitude
            corresponding to SIGMET-calculated atmospheric parameters.
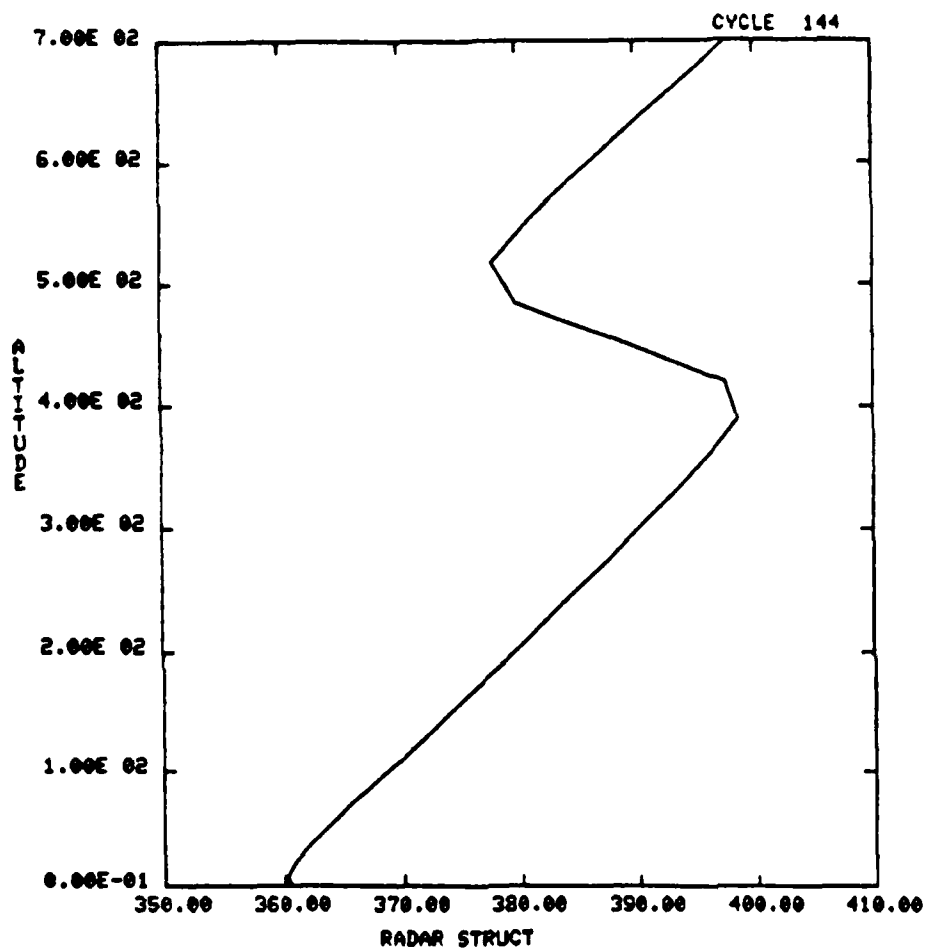   Local time = 1608 hours.

FIGURE C-3. Modified radar index of refraction as a function of altitude
corresponding to SIGMET-calculated atmospheric parameters.
Local time = 0108 hours.

D.   Internal Waves in the Marine Atmosphere

Under suitable environmental conditions the marine atmosphere will support the propagation of internal waves which may be sensed in a number of different ways. These waves provide an important mechanism for the transport of energy and momentum throughout the atmosphere, they disturb the mean flow in regions where they are generated and where they are dissipated, and they represent a systematic variability of the atmospheric state which can influence boundary layer measurements (SethuRaman, et. al., 1980).

It is of interest to study the properties of internal wave propagation as a topic of general interest in the physics of the marine atomsphere in order to assertain their rode in the processes mentioned above. More specifically, however, internal waves give rise to atmospheric disturbances which may be detected by radar; we are interested in examining whether they could offer an explanation for clear air echoes which propagate with respect to the ambient wind field. It is considered to be an established fact that large-amplitude internal waves on breaking produce patches of clear air turbulence, and it is likely that other detectable events require large amplitude waves as well.

We are not able to examine nonlinear aspects of internal wave propagation in this investigation, but the boundary layer linear perturbation calculation described in previous sections is useful for part of such a study. We can take into account the profile of stability, the effects of wind shear, and the damping by boundary layer turbulence and of convectively unstable regions. Propagation speed, camping rate, and vertical distribution of the perturbation can be calculated as functions of wavelength, propagation

direction, and mode number. It appears that the internal wave propagation problem has not been examined in this generality previously.

We have performed calculations using the PERT code, demonstrating its applicability to this class of problem. One particular case of measurements of May 16th, 1979 was chosen for study; the lower atmosphere is near neutral stability (but stable) and is capped by a more stable region. The wind direction is substantially independent of altitude, and the wind speed increases with altitude, rapidly increasing near the surface and changing more gradually in the vicinity of the inversion base. The profiles of buoyancy frequency and wind speed are shown in Fig. D-1. In this instance, the wind direction was so nearly independent of altitude that the turning with height has been neglected. The buoyancy frequency shows maxima at altitudes well above the base of the inversion; the lowest peak is at ~ 900m. Qualitatively, for large wavenumber perturbations the distrubance tends to be concentrated in the vicinity of the buoyancy peak and the phase speed is small. Calculations were carried out for this problem assuming that the turbulent dissipation is zero. Wave directions transverse to and aligned with the wind were examined. The former cases are unaffected by the wind, and form positive/negative pairs of real eigenvalues corresponding to waves traveling in opposite directions. When the waves are aligned with the wind the pairs of solutions are split apart, corresponding roughly to the augmentation of the phase speed for waves traveling down wind and a reduction of phase speed for waves traveling against the wind.

In Fig D-2 the phase speed as a function of the magnitude of the wavenumber of the perturbation is shown for the transverse case. It is

important to note that the maximum phase speed is ~ 4m/s, which is achieved
for small wavenumber and the first mode. The smallest mode number (cor-
responding to the highest frequency) will give the largest degree of ducting
of the internal wave, resulting in localization of the amplitude around the
peak of the buoyancy frequency. This tendency is illustrated in Fig. D-3
in which the amplitude of the mode 1 solution for $k = .015$ is shown.
We note that the maximum amplitude is found near the height of the peak of
buoyancy frequency, and that the wave is substantially confined to the region
of large buoyancy frequency. For this case, however, the phase speed is
no larger tham .7m/s, which is considerably smaller than the observed
disturbance speeds. With decreasing wavenumber the phase speed increases
at the same time that the internal wave occupies a wider channel. We find
that the wave is still substantially confined to the region above the base
of the inversion for a wavenumber as small as .004 (wavelength ~1500m.),
for which the phase speed is ~2m/s. This speed is still rather small, and
it is difficult to raise it appreciably for the case in question. We have
already chosen the fastest (the fundamental) mode and we quote the phase
speed rather than the group speed. Higher speeds in general are achieved
by a larger buoyancy frequency, by longer wavelengths of disturbance,
and by a deeper stable zone of the atmosphere. For longer wavelengths
for our case, however, we tend to spread the internal wave amplitude through-
out the boundary layer thickness, and it would be necessary to invoke a
mechanism (such as shear instability) for creating turbulence near the
inversion base.

In Fig. D-4 the corresponding results for phase speed vs. wavenumber
are shown for the internal waves oriented parallel or anti-parallel with

the wind. Waves having low mode number propagating with the wind are
primarily doppler shifted to a phase speed higher by approximately 4m/s.
At higher wavenumbers the effects of the terms containing wind curvature
and slope become significant, resulting in a smaller decrease in phase
speed. For waves propagating against the wind direction the dispersion
curve shows larger departures from the zero-wind case. Fig D-4 indicates
that, in addition to a general displacement upwards by ~ 4m/s of the negative
phase speed modes, there is considerable re-ordering and changing of shape
of the dispersion curves. Some mode crossing cases occur, and, in contrast
to the transverse wave cases, the imaginary part of the frequency is not
zero. Due to the two-peaked structure of D-1, it is qualitatively reasonable
to expect some mode crossing due to resonance between the two propagation
channels. And it is also possible that there may be shear-unstable modes
in this case. However, the anti-parallel modes almost invariably satisfy
conditions for critical level occurrence. It is possible, due to the
coarse zoning in the vertical, that these cases void catastrophic growth
(and absorption), but are nonetheless inaccurate (most of the critical levels
will occur near the surface where the amplitude frequently is otherwise
small). We have not explored this question in sufficient detail to evaluate
the effect of the critical levels on internal waves propagating against
the wind.

In order to evaluate the effect of turbulent dissipation and to take
a step toward treating critical levels more accurately a qualitative
study of the effects of the dissipation terms was made. We may anticipate
the trends resulting from dissipation. For a strongly stable atmosphere
dissipation will be localized near the surface where wind shear produces

a source of turbulence. Internal waves having appreciable amplitude at low altitudes will be damped while waves which are confined to elevated regions of large stability will be much less affected. Consequently, waves originating in a distant source will be filtered so that waves of higher frequency predominate. We also expect that critical layer absorption will affect the propagation of the high frequency waves traveling in the upwind direction when the profile of the wind speed results in a zone of vanishing intrinsic frequency. In this case the waves exhibit fine structure near the critical level and enhanced dissipation occurs. We have made one calculation which accounts qualitatively for dissipation by introducing a height-independent diffusivity having a magnitude of $2m^2/s$, corresponding to a stably stratified atmosphere. The dispersion calculations for aligned internal wave propagation were repeated with this addition. The real phase speed vs. wavenumber is shown in Fig D-5; comparison with D-4 indicates that dissipation has a significant effect on phase speed. While the lower modes propagation with the wind are scarcely affected, the up-wind modes are substantially changed. We also examined the imaginary parts of the frequency and found that no growing modes are present, and that significant wave decay takes place. For the down-wind modes the decay is not large; the first mode, for example, has a 3-hour e-folding decay time for $k = .006$ and longer lifetime for longer wavelengths. Higher modes decay somewhat faster. The up-wind modes, on the other hand, are strongly damped; the lowest phase speed mode for $k = .006$ decays in a few minutes, although some of the higher modes, paradoxically, decay more slowly. Although we have not explored this behavior systematically, the behavior suggests that the diffusion terms have the effect of providing the damping required to dis-

sipate internal wave energy at the critical levels.

Finally, the dependence on internal wave direction was calculated for the case k = .001 and a diffusivity of $K = 2m^2/s$. In Fig. C-6 the phase speed of the first two modes are plotted as a function of angle, ranging from the transverse direction to the down wind direction. The phase speeds each shift by ~ 4m/s as expected from the doppler shift. The maximum phase speed of these waves is not much larger than 4m/s. The effect of wave direction is to orient the waves with respect to the wind so that higher or lower phase speeds are attained. Turbulent dissipation preferentially damps the higher mode and up-wind traveling waves. The low mode waves with component of wave number in the down-wind direction have longer lifetimes; the longer wavelengths can survive many hours, but those of short wavelength have an e-folding decay time of ~ 1 hour.

The study of internal wave propagation using the linear perturbation equations provides information on the characteristics of waves favored by environmental parameters. For the case investigated in our example we have calculated the dispersion relation and the vertical distribution of the amplitude of internal waves having a range of horizontal wavenumbers. The technique could also be applied to other profiles of windspeed and lapse rate to determine the dependence on these parameters. In particular, the additional damping due to an unstable region of the buoyancy profile could be evaluated.
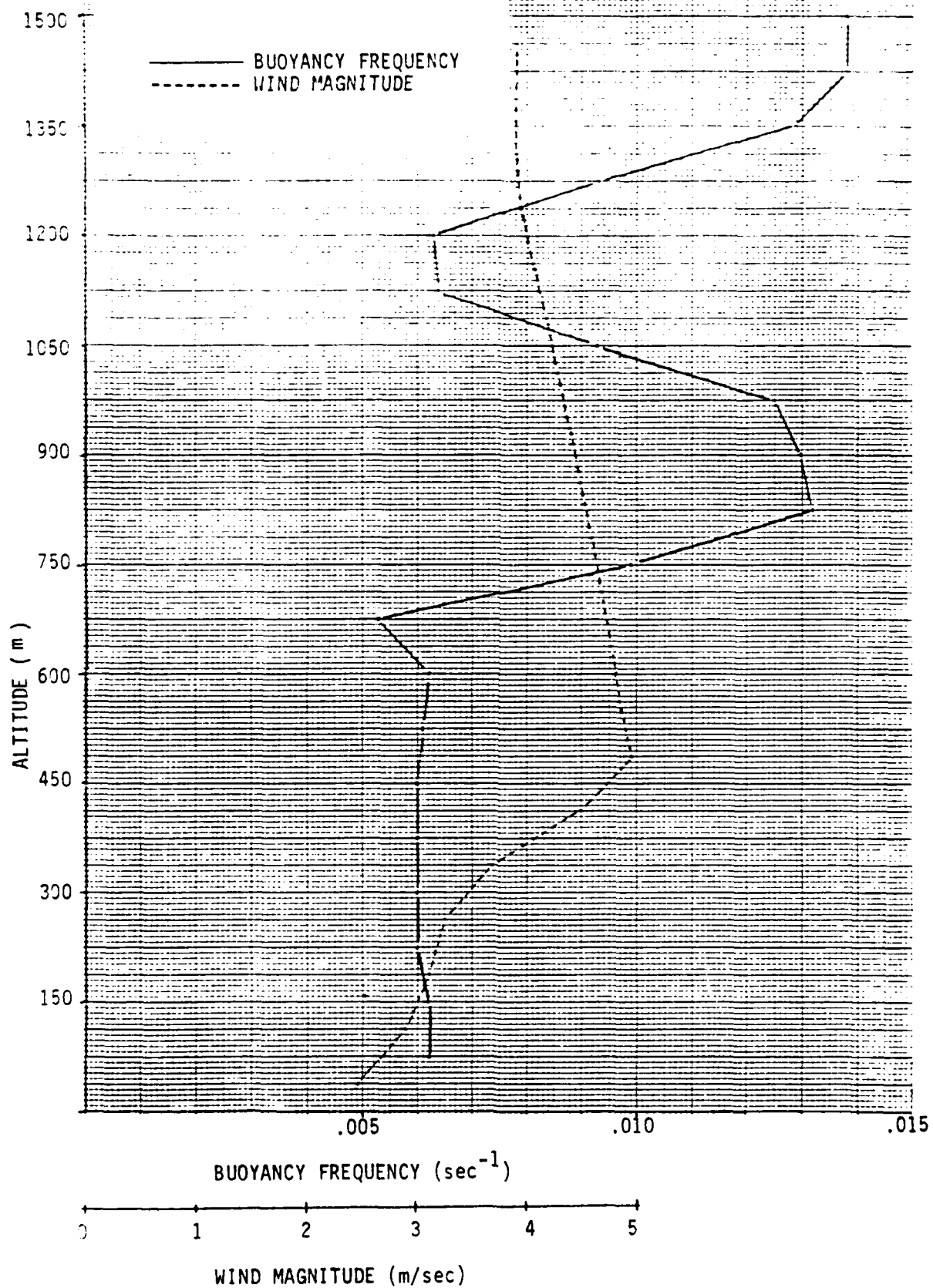
FIGURE D-1. Buoyancy frequency and magnitude of wind velocity as a function of altitude for May 16, 1979 observed data.
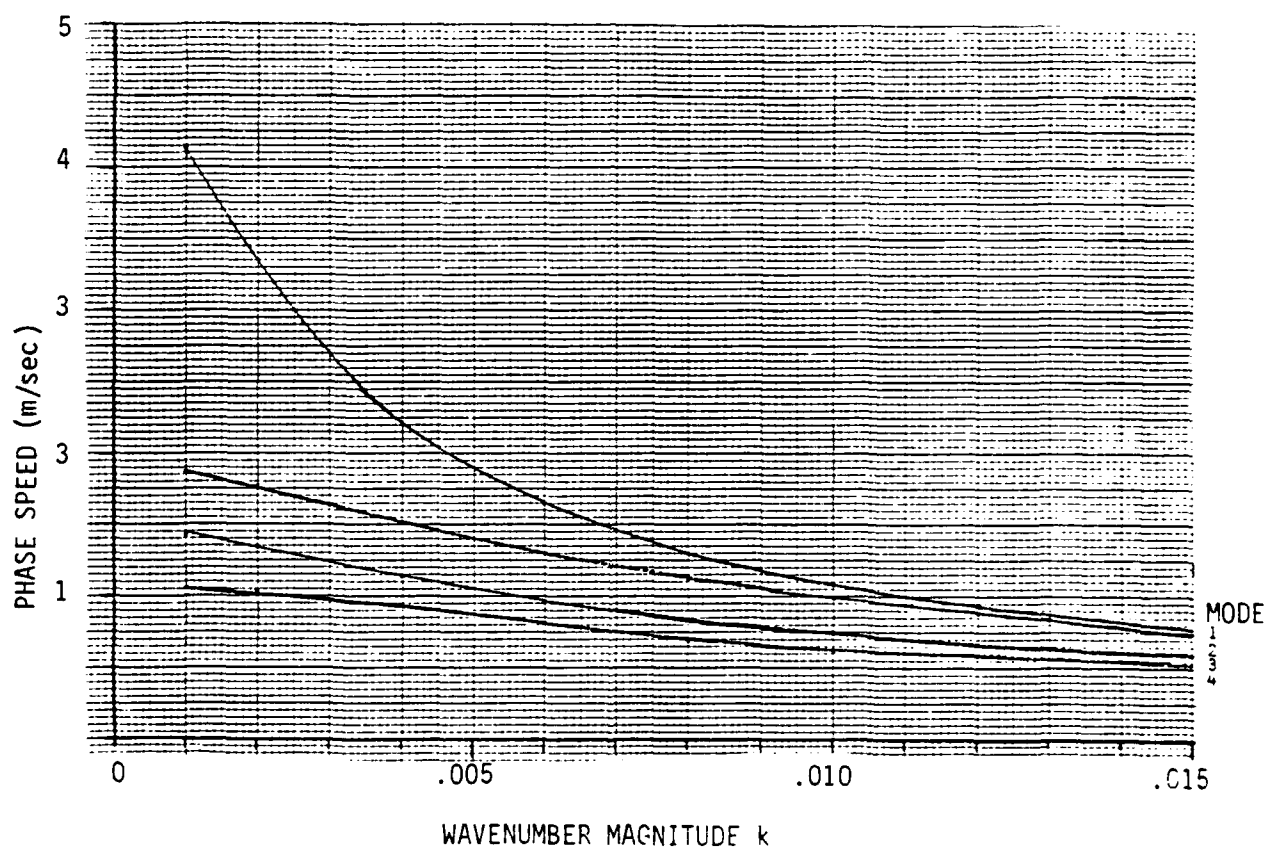
76

FIGURE D-2. Internal wave phase speed as a function of wavenumber magnitude for May 16, 1979 observed data. Wave direction transverse to wind, viscosity = 0.0.
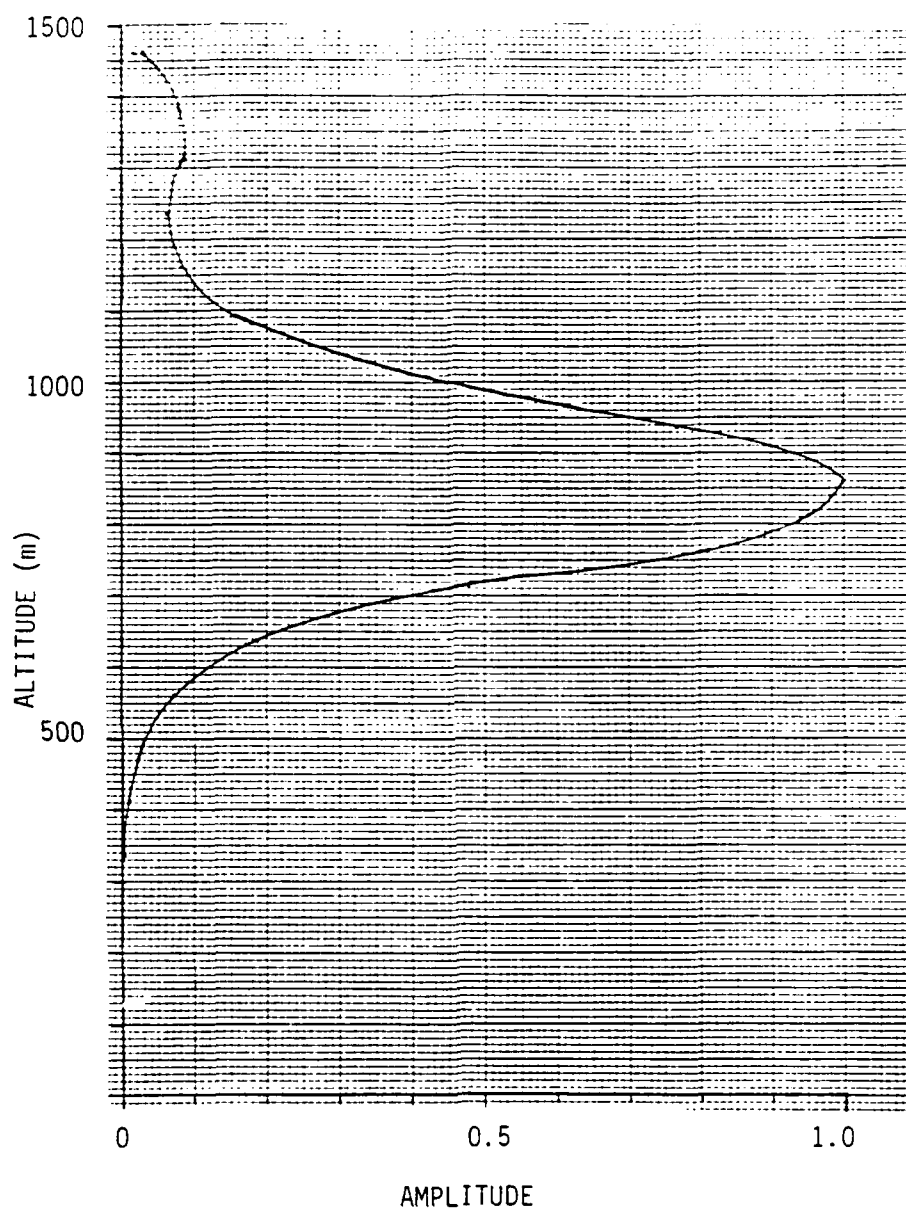
FIGURE D-3 Normalized mode 1 eigenfunction for May 19, 1979 observed data. Wave direction transverse to wind, viscosity = 0.0, |k| = 0.015.
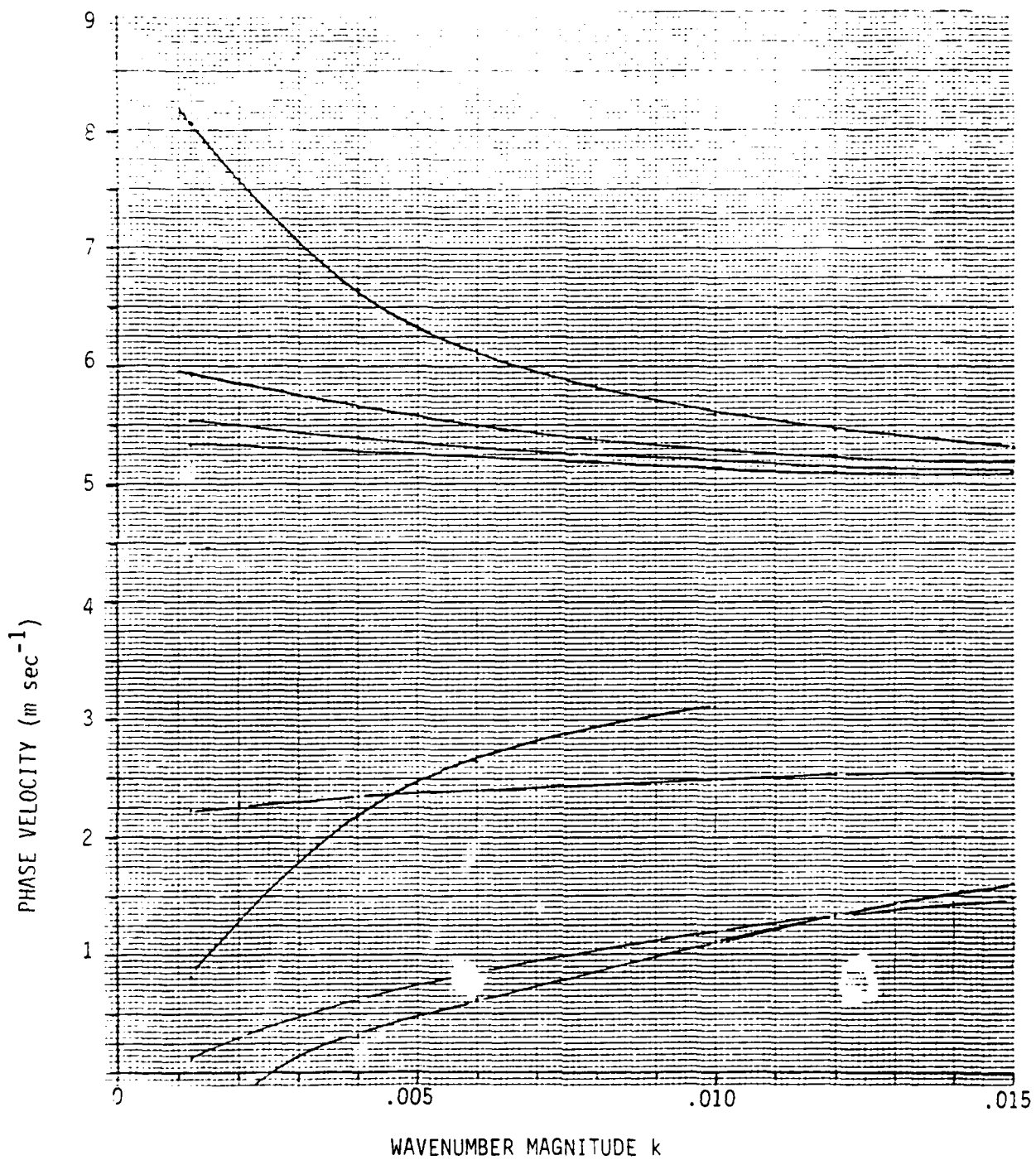
FIGURE D-4. Internal wave phase speed as a function of wavenumber magnitude for May 16, 1979 observed data. Wave direction along the wind, viscosity = 0.0.
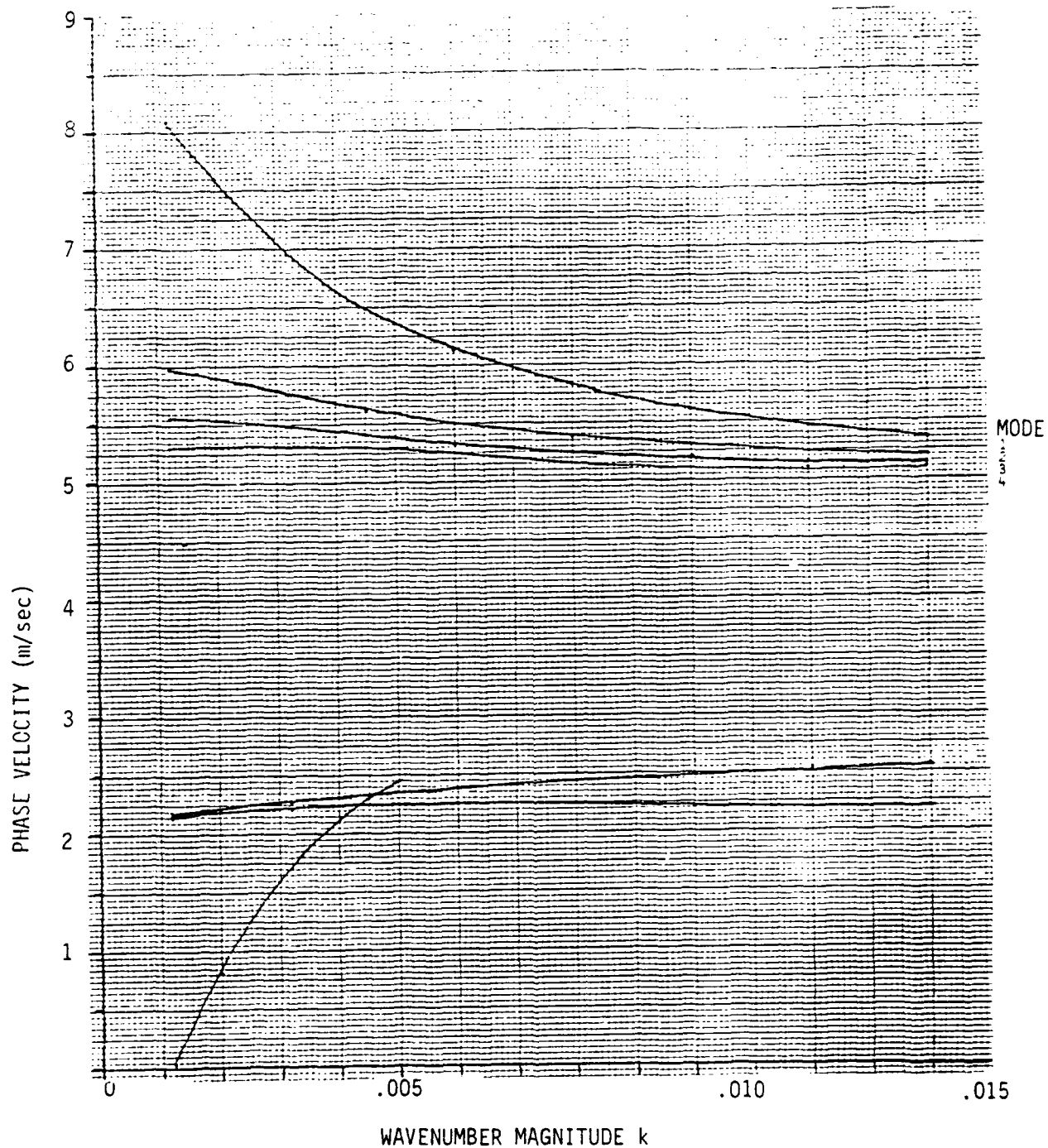
FIGURE D-5. Internal wave phase speed as a function of wavenumber magnitude for May 16, 1979 observed data. Wave direction along the wind, viscosity = 2.0 m/sec².
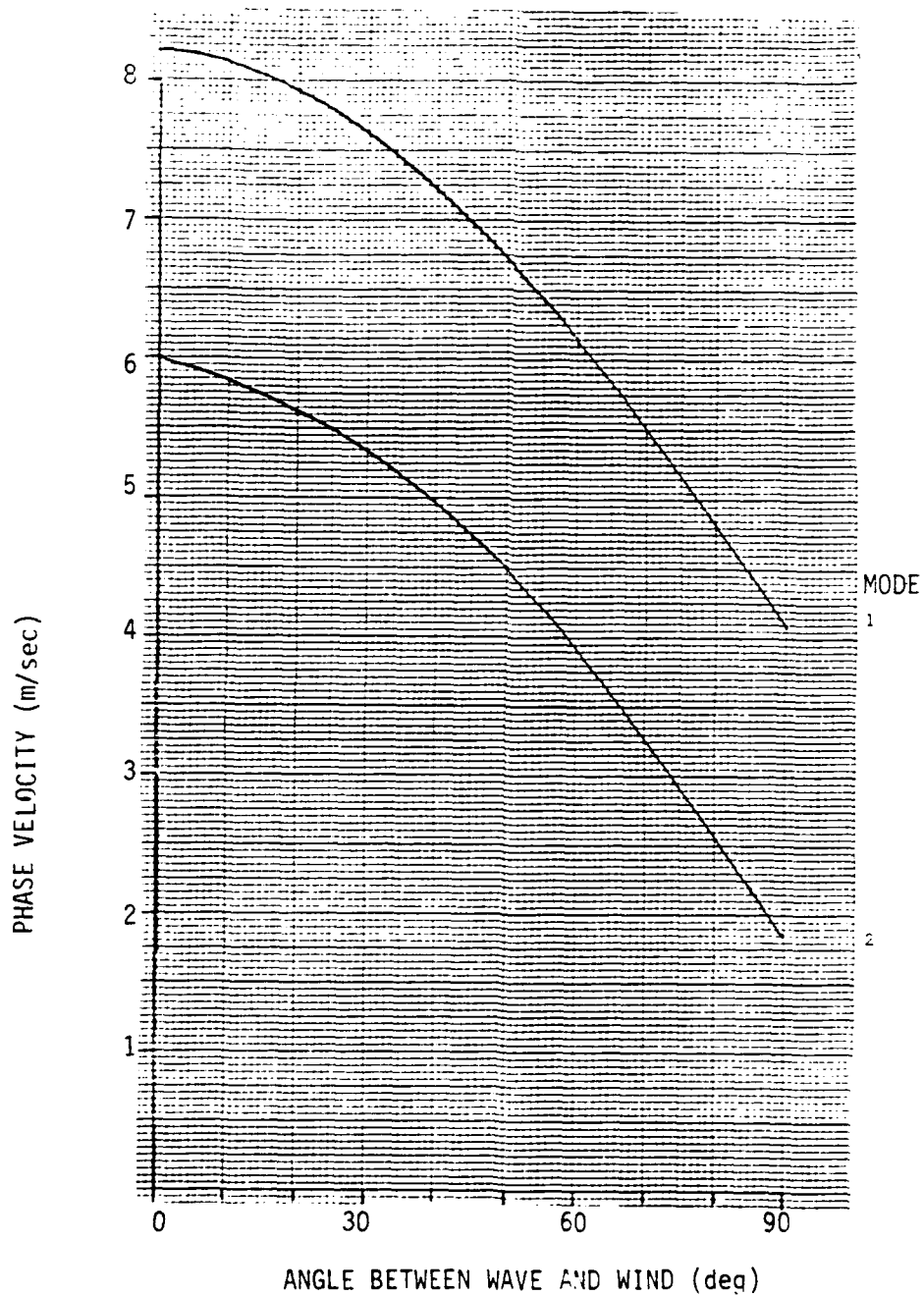
FIGURE D-6. Internal wave phase speed for modes 1 and 2 as a function of angle between wave direction and wind direction for May 16, 1979 observed data. $k = 0.001$, viscosity = 2.0 m/sec^2.

Summary and Concluding Remarks

The second phase of our "Investigation of Convective Instability in the Marine Boundary Layer" has been completed. The principal objective of this study has been to develop a quantitative boundary layer analysis technique requiring a small development effort and having low computing demands. Secondary objectives have been to consult with Naval Research Laboratory personnel on the design and interpretation of marine atmospheric measurements, and to improve understanding of marine convective phenomena as sensed by radar.

A special report was submitted outlining considerations of a theoretical nature in the conduct of marine atmospheric experiments and two visits to the Naval Research Laboratory were made to discuss current problems with laboratory personnel. The remaining topics are reported in this document where they have been organized into the four sections discussed above.

In Section A the mean structure of the boundary layer as displayed by the SIGMET computer code is discussed; in Section B, the formulation and mathematical implementation of a computer code and numerical studies of the marine boundary layer are presented. This section contains the major development of the study. In Section C, radar properties of the marine atmosphere are reviewed and in Section D a study of atmospheric internal wave propagation is reported.

The tools resulting from this investigation and previous work on atmospheric boundary layer modeling form a coordinated set having broad applications. The SIGMET boundary layer computer code takes account of the processes affecting the evolution of the profiles of density, moisture,

horizontal wind, and diffusivity in the boundary layer in response to synoptic-scale weather forcing. In addition, quantities related to the radar sensing of the atmosphere can be derived from these profiles. Finally, with the development of the linear perturbation computer code (PERT), the profiles can be employed as input data to assess wave propagation and stability of a given boundary layer. The perturbation code is sufficiently general to unify such previously diverse effects as internal wave propagation, shear layer instability, convective instability, critical layer absorption, and other various boundary layer effects leading to damping or instability.

In our investigation we have sampled a few of the applications of these codes. With the boundary layer code the modified radar index of refraction and the radar structure function were formed. A large number of perturbation calculations ($\sim$ 200) have also been carried out to test several versions of the PERT code and to investigate some new aspects of boundary layer stability. We evaluated the effect of density stratification on the Ekman unstable boundary layer taking into account the role of the Coriolis term, and we investigated the generalized dispersion relation of internal waves in a boundary layer containing a shearing wind field and turbulent dissipation. Finally, we demonstrated how the mean boundary layer code (SIGMET) and the perturbation code can be coupled together to perform a boundary layer assessment of greater generality.

Further use and development of the above tools was not possible within the scope of this investigation, but several interesting problems can be studied in the future. Particularly valuable is the possibility of correlating several different effects through the combined use of these

codes. We can determine, for example, the atmospheric conditions under which radar surface ducting takes place and the associated boundary layer stability. Another problem of interest is to determine the internal wave properties of the boundary layer for a range of weather conditions.

Clearly, a linear stability analysis reveals only one aspect of the secondary circulations of the boundary layer which result from instability. To understand the state of the atmosphere reached after these instabilities have grown requires that nonlinear effects be included. Since conventional methods of nonlinear fluid dynamics are cumbersome and very expensive, it is desirable to retain the simplicity and generality of the linear analysis in a nonlinear investigation. Some hope for accomplishing this goal is held out by expansion methods restricted to a few terms.

REFERENCES

Burk, S. D., (1980a) "Refractive Index Profile Evolution: A Numerical Model Study," Naval Environmental Prediction Research Facility, Monterey, Calif.

Burk, S.C., (1980b) "Refractive Index Structure Coefficients: Time-Dependent Calculations Using a Numerical Boundary Layer Model," to appear in $\underline{J}$. $\underline{Appl}$. $\underline{Met}$., May 1980.

Burk, S. D. (1980c) "Boundary Layer Response and Refractive Index Behavior Near Sea Surface Temperature Gradients," Second Conference on Coastal Meteorology, Los Angeles, Calif.; January 30 - February 1, 1980, p. 296 of preprints.

Francis, J.G.F., "The QR Transformation," Parts 1 and 2, $\underline{Comp}$. $\underline{Jour}$. $\underline{4}$, 265-271 (1961) and 332-345 (1962).

Freeman, B., (1978) "Formulation and Application of the Mesoscale Meteorological Simulation Model, SIGMET." Appendix of Physical Dynamics, Inc., La Jolla, Calif., Proposal PD-LJ-78-165P, submitted to the Naval Research Laboratory, Washington, D.C.

Freeman, B., (1979) "Investigation of Convective Instability in the Marine Layer (U)," Physical Dynamics, Inc., La Jolla, Calif., Report PD-LJ-79-196, Naval Research Laboratory Contract No. N00173-78-N-F133 (Secret).

Hitney, (1978) "Surface Duct Effects," Naval Ocean Systems Center, San Diego, Calif., Report No. TD144.

Lewellen, W. S., and M. E. Teske, (1975) "Development of a Low-Level Atmospheric Turbulence Model for Marine Environments," Aeronautical Research Associates of Princeton, Inc., Report 255.

Lilly, D. K., (1966) "On the Instability of Ekman Boundary Flow," $\underline{J}$. $\underline{Atmos}$. $\underline{Sci}$. $\underline{23}$, 481-494.

Milder, M., (1973) "User's Manual for the Computer Program ZMODE," R&D Associates, Santa Monica, Calif., Report RDA-TR-2701-001.

SethuRaman, S., C. Nagle, and G. Raynor, (1980) "Climatology of Internal Gravity Waves in the Marine Surface Layer in a Coastal Environment," Second Conference on Coastal Meteorology, Los Angeles, Calif., January 30 - February 1, 1980, p.244 of preprints.

Smith, B. T., $\underline{et}$ $\underline{al}$., (1976) "Matrix Eigensystem Routines: EISPACK Guide," Second Edition, New York, Springer-Verlag.